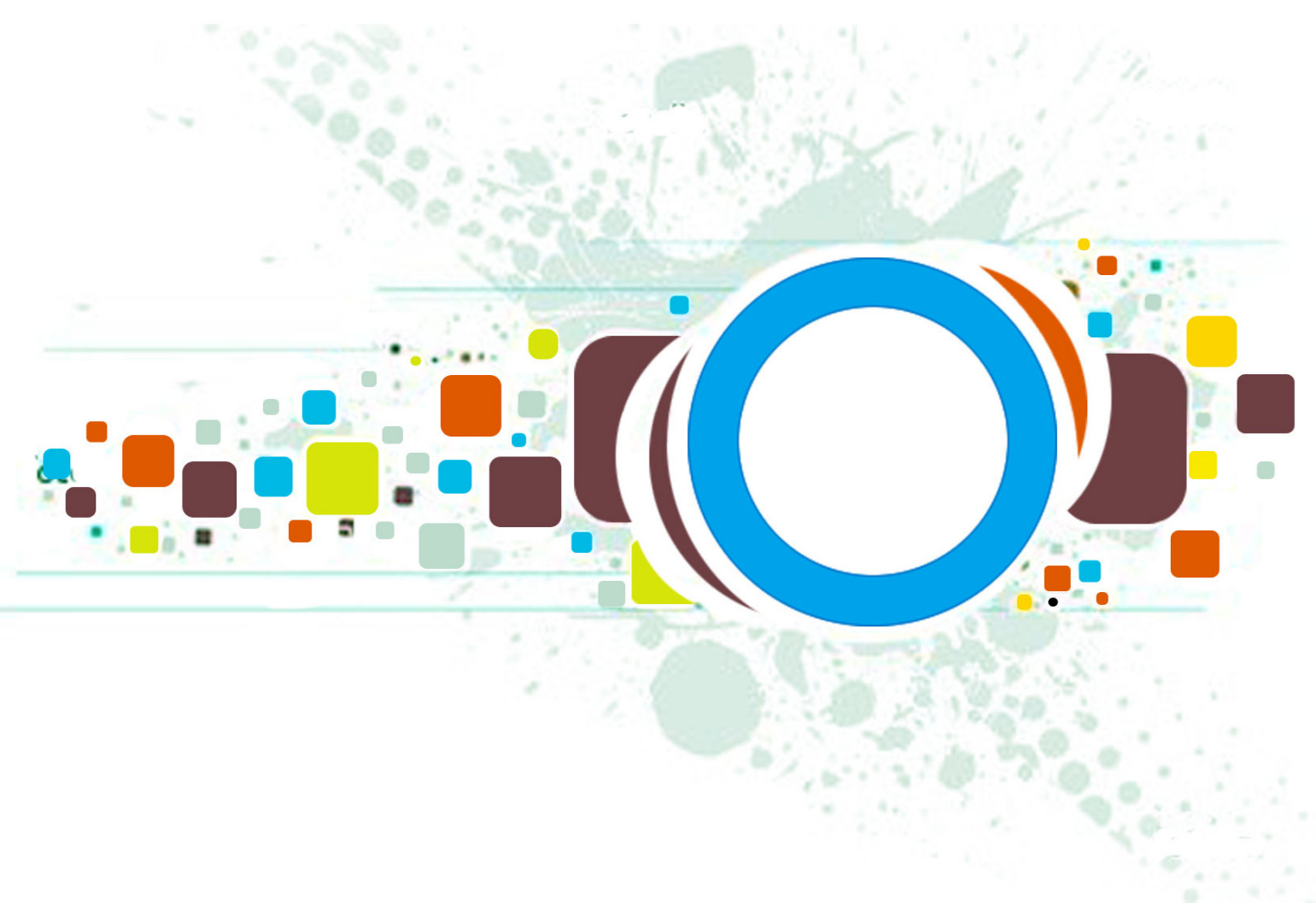


Volume 9 • Issue 5 • September / October 2015

INTERNATIONAL JOURNAL OF
IMAGE PROCESSING (IJIP)

ISSN : 1985-2304

Publication Frequency: 6 Issues Per Year



CSC PUBLISHERS
<http://www.cscjournals.org>

INTERNATIONAL JOURNAL OF IMAGE PROCESSING (IJIP)

VOLUME 9, ISSUE 5, 2015

**EDITED BY
DR. NABEEL TAHIR**

ISSN (Online): 1985-2304

International Journal of Image Processing (IJIP) is published both in traditional paper form and in Internet. This journal is published at the website <http://www.cscjournals.org>, maintained by Computer Science Journals (CSC Journals), Malaysia.

IJIP Journal is a part of CSC Publishers

Computer Science Journals

<http://www.cscjournals.org>

INTERNATIONAL JOURNAL OF IMAGE PROCESSING (IJIP)

Book: Volume 9, Issue 5, September / October 2015

Publishing Date: 31-10-2015

ISSN (Online): 1985-2304

This work is subjected to copyright. All rights are reserved whether the whole or part of the material is concerned, specifically the rights of translation, reprinting, re-use of illustrations, recitation, broadcasting, reproduction on microfilms or in any other way, and storage in data banks. Duplication of this publication of parts thereof is permitted only under the provision of the copyright law 1965, in its current version, and permission of use must always be obtained from CSC Publishers.

IJIP Journal is a part of CSC Publishers

<http://www.cscjournals.org>

© IJIP Journal

Published in Malaysia

Typesetting: Camera-ready by author, data conversion by CSC Publishing Services – CSC Journals, Malaysia

CSC Publishers, 2015

EDITORIAL PREFACE

The International Journal of Image Processing (IJIP) is an effective medium for interchange of high quality theoretical and applied research in the Image Processing domain from theoretical research to application development. This is the *Fifth* Issue of Volume *Nine* of IJIP. The Journal is published bi-monthly, with papers being peer reviewed to high international standards. IJIP emphasizes on efficient and effective image technologies, and provides a central for a deeper understanding in the discipline by encouraging the quantitative comparison and performance evaluation of the emerging components of image processing. IJIP comprehensively cover the system, processing and application aspects of image processing. Some of the important topics are architecture of imaging and vision systems, chemical and spectral sensitization, coding and transmission, generation and display, image processing: coding analysis and recognition, photopolymers, visual inspection etc.

The initial efforts helped to shape the editorial policy and to sharpen the focus of the journal. Started with Volume 9, 2015, IJIP appears with more focused issues. Besides normal publications, IJIP intends to organize special issues on more focused topics. Each special issue will have a designated editor (editors) – either member of the editorial board or another recognized specialist in the respective field.

IJIP gives an opportunity to scientists, researchers, engineers and vendors from different disciplines of image processing to share the ideas, identify problems, investigate relevant issues, share common interests, explore new approaches, and initiate possible collaborative research and system development. This journal is helpful for the researchers and R&D engineers, scientists all those persons who are involve in image processing in any shape.

Highly professional scholars give their efforts, valuable time, expertise and motivation to IJIP as Editorial board members. All submissions are evaluated by the International Editorial Board. The International Editorial Board ensures that significant developments in image processing from around the world are reflected in the IJIP publications.

IJIP editors understand that how much it is important for authors and researchers to have their work published with a minimum delay after submission of their papers. They also strongly believe that the direct communication between the editors and authors are important for the welfare, quality and wellbeing of the Journal and its readers. Therefore, all activities from paper submission to paper publication are controlled through electronic systems that include electronic submission, editorial panel and review system that ensures rapid decision with least delays in the publication processes.

To build its international reputation, we are disseminating the publication information through Google Books, Google Scholar, Directory of Open Access Journals (DOAJ), Open J Gate, ScientificCommons, Docstoc and many more. Our International Editors are working on establishing ISI listing and a good impact factor for IJIP. We would like to remind you that the success of our journal depends directly on the number of quality articles submitted for review. Accordingly, we would like to request your participation by submitting quality manuscripts for review and encouraging your colleagues to submit quality manuscripts for review. One of the great benefits we can provide to our prospective authors is the mentoring nature of our review process. IJIP provides authors with high quality, helpful reviews that are shaped to assist authors in improving their manuscripts.

Editorial Board Members

International Journal of Image Processing (IJIP)

EDITORIAL BOARD

ASSOCIATE EDITORS (AEiCs)

Professor. Khan M. Iftekharuddin
University of Memphis
United States of America

Assistant Professor M. Emre Celebi
Louisiana State University in Shreveport
United States of America

Assistant Professor Yufang Tracy Bao
Fayetteville State University
United States of America

Professor. Ryszard S. Choras
University of Technology & Life Sciences
Poland

Professor Yen-Wei Chen
Ritsumeikan University
Japan

Associate Professor Tao Gao
Tianjin University
China

Dr Choi, Hyung Il
Soongsil University
South Korea

EDITORIAL BOARD MEMBERS (EBMs)

Dr C. Saravanan
National Institute of Technology, Durgapur West Benga
India

Dr Ghassan Adnan Hamid Al-Kindi
Sohar University
Oman

Dr Cho Siu Yeung David
Nanyang Technological University
Singapore

Dr. E. Sreenivasa Reddy

Vasireddy Venkatadri Institute of Technology
India

Dr Khalid Mohamed Hosny
Zagazig University
Egypt

Dr Chin-Feng Lee
Chaoyang University of Technology
Taiwan

Professor Santhosh.P.Mathew
Mahatma Gandhi University
India

Dr Hong (Vicky) Zhao
Univ. of Alberta
Canada

Professor Yongping Zhang
Ningbo University of Technology
China

Assistant Professor Humaira Nisar
University Tunku Abdul Rahman
Malaysia

Dr M.Munir Ahamed Rabbani
Qassim University
India

Dr Yanhui Guo
University of Michigan
United States of America

Associate Professor András Hajdu
University of Debrecen
Hungary

Assistant Professor Ahmed Ayoub
Shaqra University
Egypt

Dr Irwan Prasetya Gunawan
Bakrie University
Indonesia

Assistant Professor Concetto Spampinato
University of Catania
Italy

Associate Professor João M.F. Rodrigues
University of the Algarve
Portugal

Dr Anthony Amankwah
University of Witswatersrand
South Africa

Dr Chuan Qin
University of Shanghai for Science and Technology
China

AssociateProfessor Vania Vieira Estrela
Fluminense Federal University (Universidade Federal Fluminense-UFF)
Brazil

Dr Zayde Alcicek
firat university
Turkey

Dr Irwan Prasetya Gunawan
Bakrie University
Indonesia

TABLE OF CONTENTS

Volume 9, Issue 5, September / October 2015

Pages

- 254 - 271 Fingerprint Registration Using Zernike Moments : An Approach for a Supervised Contactless Biometric System
Tahirou DJARA, Marc Kokou ASSOGBA, Amine NA IT-ALI, Antoine VIANOU
- 272 - 282 Robust Digital Image Watermarking Technique in DWT domain based on HVS and BPNN
Jagadeesh Bandi, P. Rajesh Kumar, P. Chenna Reddy
- 283 - 303 Hybrid Domain based Face Recognition using DWT, FFT and Compressed CLBP
Sujatha B M , K Suresh Babu, K B Raja, Venugopal K R

Fingerprint Registration Using Zernike Moments : An Approach for a Supervised Contactless Biometric System

Tahirou DJARA

csm.djara@gmail.com

*Laboratory of Electronic Engineering,
Telecommunications and Applied data Processing Technology.
Ecole Polytechnique of Abomey Calavi (EPAC).
University of Abomey-Calavi. 01 BP 2009 Cotonou, BENIN.*

Marc Kokou ASSOGBA

mkokouassogba@yahoo.fr

*Laboratory of Electronic Engineering,
Telecommunications and Applied data Processing Technology.
Ecole Polytechnique of Abomey Calavi (EPAC).
University of Abomey-Calavi. 01 BP 2009 Cotonou, BENIN.*

Amine NAÏT-ALI

amine.naitali@gmail.com

*Laboratory Images, Signals and Intelligent Systems
University of Paris Est-Créteil,
122, rue Paul Armangot, 94400 Vitry sur Seine*

Antoine VIANOU

avianou@yahoo.fr

*Laboratory of Electronic Engineering,
Telecommunications and Applied data Processing Technology.
Ecole Polytechnique of Abomey Calavi (EPAC).
University of Abomey-Calavi. 01 BP 2009 Cotonou, BENIN.*

Abstract

In this work, we deal with contactless fingerprint biometrics. More specifically, we are interested in solving the problem of registration by taking into consideration some constraints such as finger rotation and translation. In the proposed method, the registration requires: (1) a segmentation technique to extract streaks, (2) a skeletonization technique to extract the center line streaks and (3) and landmarks extraction technique. The correspondence between the sets of control points, is obtained by calculating the descriptor vector of Zernike moments on a window of size $R \times R$ centered at each point. Comparison of correlation coefficients between the descriptor vectors of Zernike moments helps define the corresponding points. The estimation of parameters of the existing deformation between images is performed using RANSAC algorithm (Random Sample Consensus) that suppresses wrong matches. Finally, performance evaluation is achieved on a set of fingerprint images where promising results are reported.

Keywords: Contactless Biometry, Fingerprint, Zernike Moments, Image Registration.

1. INTRODUCTION

Due to its unicity, fingerprint is probably one of the most common modality used to identify individuals[1]. However, classical fingerprint devices requiring a direct contact (touch-based) have some main drawbacks related to acquisition conditions such as: eventual elasticity of the finger, environment conditions, hygiene problem (i.e. same sensor touched by users) that can be particularly exacerbated during the outbreak of epidemics or pandemics. To overcome these problems, contactless based-systems seem to be much more appropriate and useful as stated by the US Department of Homeland Security (DHS) which considers that the development of a Biometric Detector prototype capable for acquiring contactless fingerprint for identity

management will improve fingerprint acquisition quality and recognition and reduce false positives [2].

Fingerprint registration is a critical step when dealing with fingerprint matching. The registration is a classic problem in computer vision that occurs in many tasks of analysis and image processing. Every method should take into account not only the assumed type of geometric deformation between the images but also radiometric deformations and noise corruption, required registration accuracy and application-dependent data characteristics [3].

The goal of an algorithm for image registration is to match images 2D or 3D so as to overlay the pixels or voxels representing the same structures. Our method consists in determining the transformation linking the bifurcation points contained in an image to readjust and its correspondence on the other anatomical image (called reference image) as shown in figure 1.

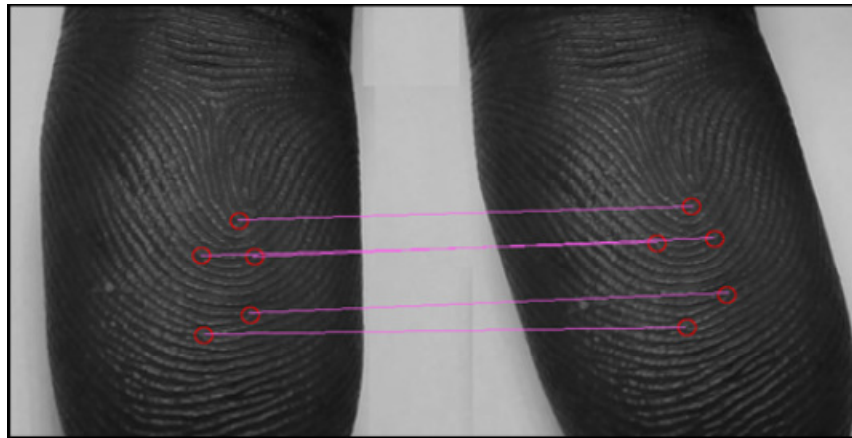


FIGURE 1: Determination of Corresponding Bifurcation.

Although a variety of registration alignment algorithms have been proposed, accurate fingerprint registration remains an unresolved problem [4]. Based on the features that the matching algorithms use, fingerprint matching can be classified into image-based and graph-based matching [5].

Image-based matching [6] uses the entire gray scale fingerprint image as a template to match against input fingerprint images. The primary shortcoming of this method is that matching may be seriously affected by some factors such as image quality variation, and distortion, which are inherent properties of contact fingerprint images.

Graph-based matching [7, 8] represents the minutiae in the form of graphs. The high computational complexity of graph matching hinders its implementation. For instance, in [9] proposed algorithms for matching fingerprints using the relative position of minutiae whose implementation is relatively simple.

In this work, fingerprints are acquired using a simple camera. For registration purpose, we present an approach that deals with minutia for the matching process, combined with techniques developed in [10, 11]. More specifically, we show how one can use Zernike moments for an efficient registration.

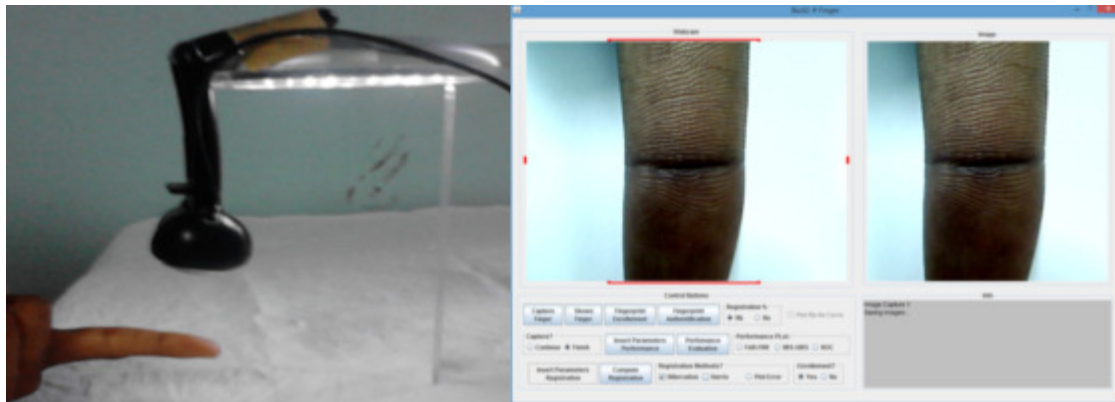
This paper is organized as follows: in section 2 we present the experimental condition. The proposed method is presented in section 3. Section 4 contains the discussion about the experimental results, and finally; we conclude our work in section 5.

2. EXPERIMENTAL CONDITIONS

In the literature, there are few studies focused on contactless systems [12, 13]. Most systems require the placement of the finger on predisposed guides in order to simplify the image acquisition step [12, 14]. Experiments are carried out in [12, 15, 16] with different distances and resolution for contactless image acquisition.

2.1 Acquisition Protocol

The contactless fingerprint acquisition system which we are presenting is a part of [12, 14]. We have developed a Contactless Biometric Fingerprint Software (CBFS) for the acquisition and processing our images. It implements our method of fingerprint registration. The contactless fingerprint acquisition system we present consists of this CBFS (Figure 2.b) to visualize the sharpness of the images before capture, a webcam for taking digital photo, and lighting equipment (Figure 2.a). The user is prompted to place the reverse of his finger on a desk. The palm of the user is faced with the webcam. We proceed to the capture of fingerprint. In order to limit travel, a rectangular area is defined on the interface of the webcam which will contain the finger before capture.



(a) Acquisition system

(b) The portal of the software

FIGURE 2: Contactless fingerprint acquisition system and Screenshot of CBFS.

2.2 Pre-Processing Phase

The pre-processing phase plays a significant role in improving the image contrast. The contrast enhancement is used to reduce the imperfection which generally occurred due to sensor noise or inconsistent illumination. Histogram equalizing method is used to adjust the distribution of grayscale.

3. PROPOSED METHOD

We have developed a method to proceed with registration of fingerprint images. This registration method aims at determining the $\emptyset = (t_x, t_y, \theta_{xy})^t$ parameters of 2D translation and rotation. Under experimental conditions, our images are obtained at a fixed distance from the sensor, therefore the scale factor is not taken into account.

The proposed registration method is performed in five steps that are detailed as follows:

- Step 1.** Image segmentation and skeletonization to extract center line (cl) streaks,
- Step 2.** Automatic selection a set of control points to be matched from the reference image and the input image,
- Step 3.** Description of each image using Zernike moments,
- Step 4.** Definition of a similarity measure to establish a correspondence between the detected corresponding points from the two images,

Step 5. Estimation of parameters that model the best deformation between sets..

3.1 Segmentation

Segmentation is the process of separating foreground regions in an image from background regions. The foreground regions correspond to the clear fingerprint area containing ridges and valleys, which is the area of interest. The background corresponds to the regions outside the borders of the fingerprint area, which do not contain any valid fingerprint information. In our method, we first eliminate the background regions that allow us to obtain an image of the foreground regions (FR). In a second step, the ridges are extracted from FR.

3.1.1. Foreground Regions Extraction

The extraction of streaks is linked to the extraction of foreground regions. For this purpose, we have applied a filter to the image in order to define its contour. Then a binary mask is subsequently applied to the image filter, which allows to have an image defining the contour of the fingerprint. This contour image is used for the extraction of foreground regions.

3.1.2. Streaks Extraction

In order to get the streaks in the image of fingerprint, a photometric adaptive threshold method has been developed [17]. Two thresholds are defined i.e. S_s and S_h corresponding to the mean of a square framework and the mean of a hexagonal framework.

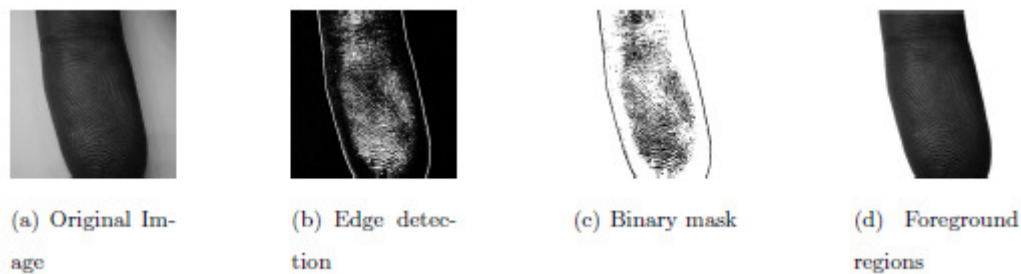


FIGURE 3: Main steps of the extraction of the foreground regions.

A pixel $P(x, y)$ is deleted or not by comparing its value with S_s and S_h . Photometric thresholding being preceded by the extraction of the region of interest. The streaks image is skeletonized in order to get minutiae i.e. streak ending points and streak bifurcation points.

3.2 Automatic Selection of Landmarks

The first step in a process of automatic image registration of fingerprints involves the automatic selection of a set of potential control points from two images F_t and F_{t+d} to realign. The performance at this stage of selection of control points is important because it depicts the quality of registration.

Control points, which should serve as a pivot for distortion correction must be sure points. They must be easily identifiable landmarks and intangible. In [10, 11], an automatic extraction of Landmark-based NSCT (No Sub-sampled Contourlets Transform) has been suggested.

It should be noted that in the case of fingerprint images, the points that naturally characterize them are minutiae. Termination and bifurcation type minutiae are mainly the signature of a fingerprint [18].

We have used the bifurcation points extracted from the algorithm presented in [19] and used in [20] for the detection of minutiae of a fingerprint image.

3.3. Zernike Moments Calculation

3.3.1. Definition and Properties of Zernike Moments

In (ρ, θ) polar coordinates, the Zernike radial polynomials of order p with repetition q are defined by [21]:

$$R_{pq}(\rho) = \sum_{s=0}^{\frac{p-|q|}{2}} \frac{(-1)^s (p-s)!}{s! \left(\frac{p+|q|}{2} - s\right)! \left(\frac{p-|q|}{2} - s\right)!} \rho^{p-2s} \quad (1)$$

In the above equation p is a non-negative integer, ($p \geq 0$), and q positive and negative integers subject to the constraints:

$$\begin{cases} p - |q| \text{ is even} \\ |q| \leq p \end{cases} \quad (2)$$

The Zernike moment of order p with repetition q for a continuous image function $f(x, y)$, that vanishes outside the unit disk is:

$$Z_{pq} = \frac{p+1}{\pi} \iint_{x^2+y^2 \leq 1} V_{pq}^*(\rho, \theta) f(x, y) dx dy \quad (3)$$

For the digital image, the integrals are replaced by summations [22] to get :

$$Z_{pq} = \frac{p+1}{\pi} \sum_x \sum_y V_{pq}^*(\rho, \theta) F(x, y) \quad (4)$$

with

$$V_{pq}(\rho, \theta) = R_{pq}(\rho) e^{iq\theta} \quad (5)$$

where V_{pq}^* denote complex conjugate of V_{pq} , $\rho = \sqrt{x^2 + y^2} \leq 1$ and $\theta = \tan^{-1}\left(\frac{y}{x}\right)$.

The computation of radial Zernike polynomial $R_{pq}(\rho)$ is performed according to a recursive algorithm [21, 23] by replacing the index $p - 2s$ by k in equation (1). We can rewrite the radial polynomials in powers of k as follows :

$$R_{pq}(\rho) = \sum_{k=|q|}^p B_{pqk} \rho^k, (p - k \text{ is even}) \quad (6)$$

where

$$B_{pqk} = \frac{(-1)^{\frac{p-k}{2}} \left(\frac{p+k}{2}\right)!}{\left(\frac{p-k}{2}\right)! \left(\frac{k+|q|}{2}\right)! \left(\frac{k-|q|}{2}\right)!} \quad (7)$$

Equation (6) is generally preferred to equation (1) for the evaluation of the Zernike polynomials [24]. A study [25] has shown that Zernike moments are less sensitive to noise and less redundant information. Many works like [21, 26] were then performed on the invariance of the moments considering the affine transformation coordinates and intensity changes in grayscale images.

The defined features of Zernike moments themselves are only invariant to rotation. To obtain scale and translation invariance, the image needs to be normalized first by using the regular Zernike moments. Zernike features invariant to translation are then extracted from the normalized image [27].

3.3.2. Zernike Moments on Binary two Fingerprints

Figure 5 shows the Zernike moments computed on binary fingerprint images presented in Figure 4. Image 2 is the 180° rotation version of image 2. One can notice that for the two images, we have similar values of Zernike moments. This shows the invariance of Zernike moments in rotation.

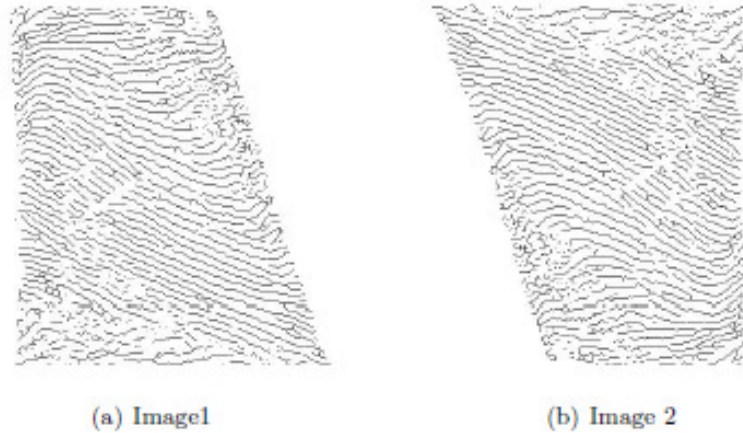


FIGURE 4: Two binary images of fingerprints different of 180°.

Image1		Image 2 : Image 1 rotated	
pq	$ Z_{pq} $	pq	$ Z_{pq} $
00	0.2893952	00	0.2893952
11	0.0058495	11	0.0058495
20	0.1317473	20	0.1317473
22	0.1051705	22	0.1051705
31	0.0147638	31	0.0147638
33	0.0579088	33	0.0579088
40	0.0547054	40	0.0547054
42	0.0225529	42	0.0225529
44	0.0536853	44	0.0536853
51	0.0009113	51	0.0009113
53	0.0181444	53	0.0181444
55	0.0225388	55	0.0225388

TABLE 1: Module of Zernike moments of two binary fingerprints images different of 180°.

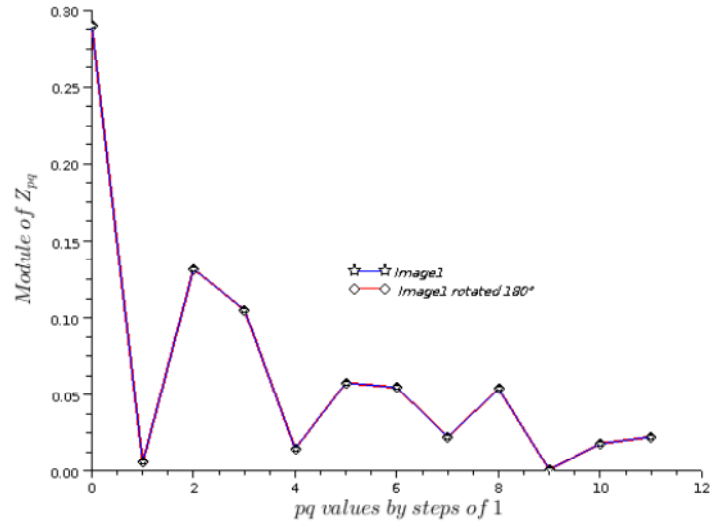


FIGURE 5: Zernike moments applied to the binary image of the Figure 4.

3.4. Matching Process

After extraction of bifurcation points on the cl of realign images to readjust, we are left with two sets of points to match : a set of bifurcation points on the reference image F_t and a set of bifurcation points on the input image F_{t+d} . The correspondence between these two sets of control points is obtained by following steps:

- ✓ Subdivide each image into thumbnail size $L \times L$ centered on each point bifurcations B_i .
- ✓ For each thumbnail centered on this point B_i , construct the descriptor vector of Zernike moments M_z as follows:

$$P_z = (|Z_{11}|, \dots, |Z_{pq}|, \dots, |Z_{55}|) \tag{8}$$

where $|Z_{pq}|$ is the module of Zernike moments. We have used as the highest order of moments 5 after several experimental trials. Although the higher order moments are the fine details of the image, they are more sensitive to noise than lower order moments.

- ✓ For any point r_i of the reference image, we suppose that its corresponding e_i of input image is from a set of points on F_{t+d} . located within a certain radius R' around r_i . The radius R' limits the search for corresponding and therefore, reduces the number of comparisons to achieve in order to find out the corresponding points.

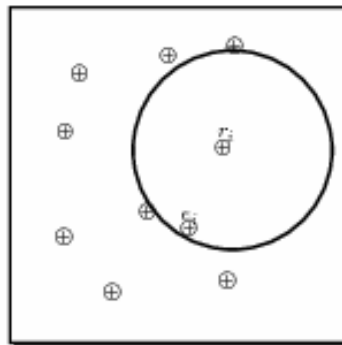


FIGURE 6: Determining the corresponding e_i (of input image F_{t+d}) of a bifurcation point r_i (of the reference image F_t).

- ✓ The matching process is performed by calculating the correlation coefficients between the two vectors descriptors. The corresponding points are those which give the maximum value of correlation coefficient.

The correlation coefficient between two vectors of the feature $X(x_1, \dots, x_n)$ and $Y(y_1, \dots, y_n)$ is given by the following formula:

$$C = \frac{\sum_{i=1}^n (x_i - \bar{x}) \cdot (y_i - \bar{y})}{\sqrt{\sum_{i=1}^n (x_i - \bar{x})^2} \cdot \sqrt{\sum_{i=1}^n (y_i - \bar{y})^2}} \quad (9)$$

where \bar{x} and \bar{y} are averages of the two vectors X and Y respectively.

If C is 0, the two vectors are not correlated. The two vectors are even better correlated than C is far from 0 (near -1 or 1).

3.5. Estimation of the Registration Geometric Transformation

Once the information type to be used to guide the registration and the similarity criterion quantifying the similarity between two images are defined, the model of deformation is determined to realign the images. The choice of the model of deformation is very important and is guided by the underlying application and the information, at first instant, available about the nature of the deformation between the images.

The geometric transformations or deformation models involved in the registration of 2D images are generally of rigid, affine or curvilinear [28].

3.5.1. Rigid Transformation

A registration transformation is rigid when it conserves the distance between any two points. Only the rotation and translation are taken into account. Coordinates (x, y) of any point M of the image to readjust are transformed as follows :

$$\begin{pmatrix} x' - x_0 \\ y' - y_0 \end{pmatrix} = \begin{pmatrix} \cos\theta & -\sin\theta \\ \sin\theta & \cos\theta \end{pmatrix} \begin{pmatrix} x - x_0 \\ y - y_0 \end{pmatrix} + \begin{pmatrix} t_x \\ t_y \end{pmatrix} \quad (10)$$

where $M_0 \begin{pmatrix} x_0 \\ y_0 \end{pmatrix}$ is the center of rotation, θ the angle of rotation, $\begin{pmatrix} t_x \\ t_y \end{pmatrix}$ the coordinates of the translation vector and $M' \begin{pmatrix} x' \\ y' \end{pmatrix}$, the transform of M.

3.5.2. Affine Transformation

A registration transformation is affine when it preserves parallelism and takes into account the difference in scale between the images. The coordinates $\begin{pmatrix} x \\ y \end{pmatrix}$ of any point of the image to readjust are transformed as follows :

$$\begin{pmatrix} x' \\ y' \end{pmatrix} = \begin{pmatrix} a_{11} & a_{12} \\ a_{21} & a_{22} \end{pmatrix} \begin{pmatrix} x \\ y \end{pmatrix} + \begin{pmatrix} t_x \\ t_y \end{pmatrix} \quad (11)$$

with $a_{11}, a_{12}, a_{21}, a_{22}$ real coefficients and $\begin{pmatrix} t_x \\ t_y \end{pmatrix}$ the translation vector coordinates.

3.5.3. Curvilinear Transformation

A registration transformation of the curvilinear type is a polynomial function. It takes into account the distortions between the images. The coordinates $\begin{pmatrix} x \\ y \end{pmatrix}$ of any point of the image to readjust are transformed as follows :

$$\begin{cases} x' = a_{00} + a_{10}x + a_{01}y + a_{20}x^2 + a_{11}xy + a_{02}y^2 + \dots \\ y' = b_{00} + b_{10}x + b_{01}y + b_{20}x^2 + b_{11}xy + b_{02}y^2 + \dots \end{cases} \quad (12)$$

with a_{ij} , b_{ij} , real coefficients.

Figure 7 shows a practical example of the different transformations.

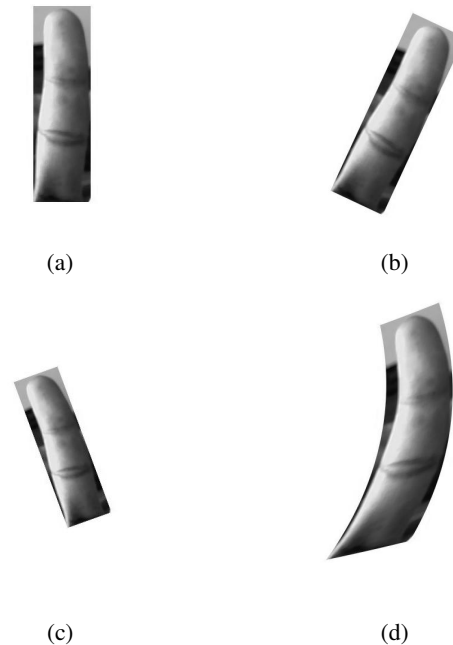


FIGURE 7: Practical examples of different types of registration geometric transformation. (a) Input image, (b) Rigid transformation, (c) Affine transformation, (d) Curvilinear transformation.

3.5.4. Deformation Model Retained

The transformation model used to produce the image distortion F_{t+d} is the rigid transformation model expressed by Equation (10). This model is appropriate for the case of our fingerprint images captured at a fixed distance from the sensor.

The estimation of the parameters of the rigid transformation is carried out iteratively. At each iteration we provide online processing parameters found by RANSAC.

The RANdom SAmple Consensus (RANSAC) is an algorithm proposed for the first time in 1981 by Fischler and Bolles [29]. It is a general parameter estimation approach designed to cope with a large proportion of outliers in the input data. This is a popular method in regression problems containing aberrant data or outliers [30].

As pointed out by Fischler and Bolles [29], unlike conventional sampling techniques that use as much of the data as possible to obtain an initial solution and then proceed to prune outliers, RANSAC uses the smallest set possible and proceeds to enlarge this set with consistent data points [29]. In [31, 32], RANSAC is used to refine the search for matching between the pores in the fingerprint identification process of individuals.

The basic RANSAC algorithm is summarized as follows :

Algorithm 1 RANSAC

- 1: Select randomly the minimum number of points required to determine the model parameters.
 - 2: Solve for the parameters of the model.
 - 3: Determine how many points from the set of all points fit with a predefined tolerance ϵ .
 - 4: If the fraction of the number of inliers over the total number points in the set exceeds a predefined threshold τ , re-estimate the model parameters using all the identified inliers and terminate.
 - 5: Otherwise, repeat steps 1 through 4 (maximum of N times).
-

The number of iterations, k , is chosen high enough to ensure that the probability p (usually set to 0.99) that at least one of the sets of random samples does not include an outlier. Let w represent the probability that any selected data point is an inlier and $\epsilon = 1 - w$ the probability of observing an outlier.

A common case is that w is not known in advance, but an approximate value can be estimated using the following algorithm [33].

Algorithm 2 : Adaptive algorithm for determining the number of RANSAC samples[33].

Require: $k = \infty$, *sample count* = 0.

- 1: **while** $k >$ *sample count* **do**
 - 2: Choose a sample and count the number of inliers
 - 3: Set $\epsilon = 1 - \frac{\text{number of inliers}}{\text{total number of points}}$
 - 4: Set k from ϵ and (13) with $p = 0.99$
 - 5: Increment the sample count by 1
 - 6: **end while**
-

According to [33, 34], the maximum number of iterations of the algorithm is given by :

$$k = \frac{\log(1-p)}{\log(1-(1-\epsilon)^n)} \tag{13}$$

where n is the size of the sample.

Figure 8, shows an example of 7 pairs of points of interest including 3 red discharged after treatment of the RANSAC algorithm.

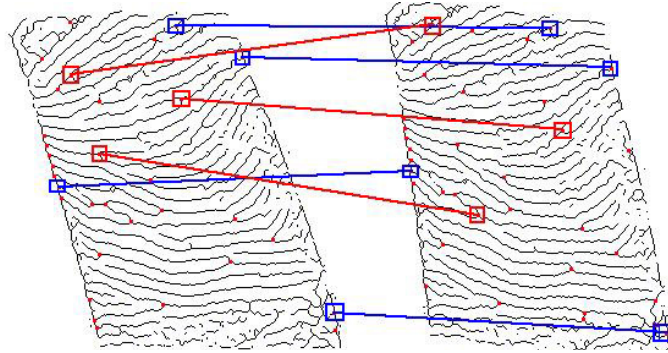


FIGURE 8: 7 pairs of correspondents found in the matching process including 3 red rejected by RANSAC.

4. Experimental Results

This section is dedicated to the validation and the evaluation of the performances of the proposed registration algorithm in terms of precision.

In order to evaluate the precision of the proposed registration algorithm, we have used a first time synthetic geometric distortion. The deformation model chosen was applied to a database of fingerprint images that we have formed. Our test image database consists of 80 grayscale images of size 480×480 pixels. Ten images are shown in Figure 9. In a second phase, we used images acquired at different times, so deformation is not known in advance. We have applied the different stages of the registration to these images.

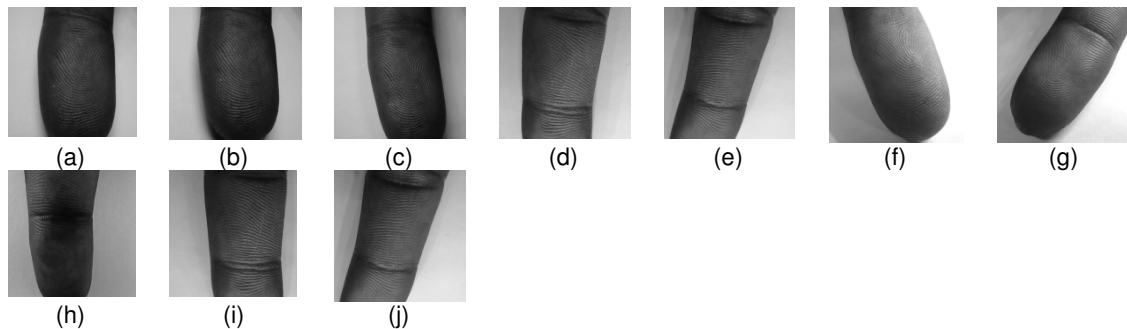


FIGURE 9: 10 images of 80 images contained in our database.

The registration method developed is based on the calculated Zernike moments in each point of interest. In the research phase of points, the introduction of the parameter limiting the search area has significantly made it possible to reduce the running time of finding a correspondent from 1106ms to 93ms.

We have written a Java code, implemented through the CBFS in order to implement the proposed method.

The first test can be described in the following steps:

1. Rotation(R) and Translation(T) transformations have been applied to the test images(I). We used the Random Java function to generate randomly for each image vector of translation and rotation. $R \in [1; 19]$ and $T \in \langle (3; 3) \dots (9; 9) \rangle$.
2. Performance analysis of the algorithm : To plot the curve of the actual parameters and the curve of the estimated parameters to show the accuracy of the algorithm.

3. Computation of error between each real parameters and its estimated parameters, using the following equation:

$$\varepsilon_i = \frac{|\theta_i - \theta'_i|}{\theta_i} \tag{14}$$

where ε_i is the error associated with estimating angles.

The second test is to work with two images acquired at different times thus deformation unknown. The test consists of following steps:

1. Estimate of the existing deformation between the two images.
2. Quantification of the precision of the estimated transformation. Here, we have measured the precision by the Root Mean Square Error (RMSE), which represents the distance between the position of a control point, once the image, is corrected, and its position on the reference image. It is given by the following formula:

$$RMSE = \sqrt{\frac{1}{M} \left(\sum_i \|(x_i, y_i) - T_{affine}^{-1}(x'_i, y'_i)\|^2 \right)} \tag{15}$$

where (x'_i, y'_i) is the correspondent of (x_i, y_i) control point of the reference image, T_{affine} is the estimated affine transformation, $\|(x_i, y_i) - T_{affine}^{-1}(x'_i, y'_i)\|$ is the euclidean distance and M is the number of interest pairs points.

Figure 10 shows the representation of real and estimated orientations of test images based on the hyperbolic cosine function:

$$f : \theta \mapsto \cosh(\theta) = \frac{e^\theta - e^{-\theta}}{2} \tag{16}$$

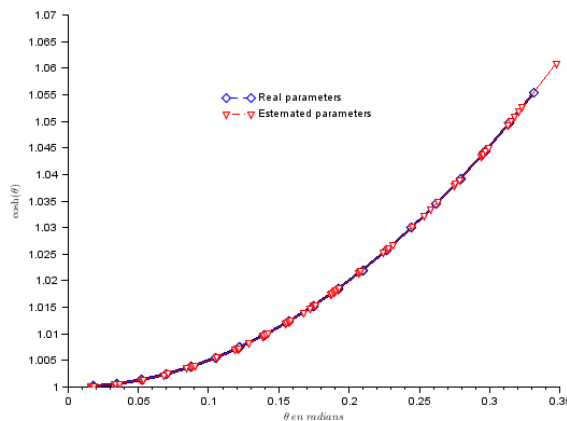


FIGURE 10: Real parameters and estimated parameters.

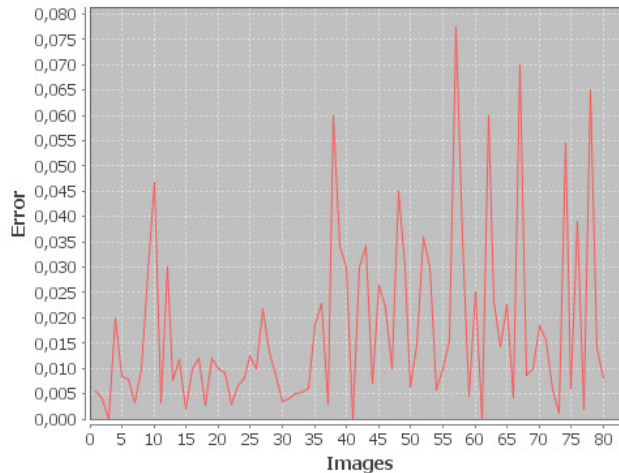


FIGURE 11: Error between original images and transformed images.

It may be noted that we have similar values between the estimated orientation and the real orientation for each image. This is confirmed by the Figure 11 which represents the relative error between the two parameters. The largest error is less than 0.08, while the smallest is about 0.

For the first test, we only show in a Figure 12 the results obtained by the proposed method in image of Figure 9-(a). The Figure 12-(d), show the result of the registration of the images in grayscale, while the Figure 12-(f) show the result of the registration Ic extracted from the images in Figure12-(a)-(b). Figure 13 shows the zoom of the framed images of Figure 12-e and 12-f.

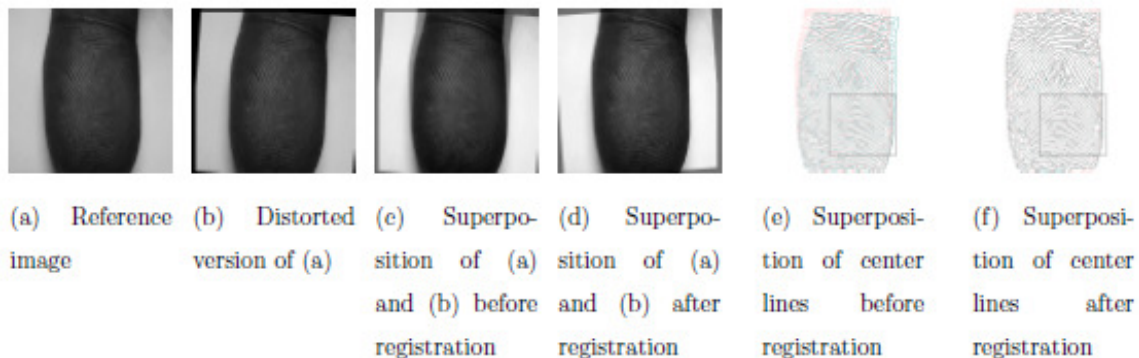


FIGURE 12: Result of registration. The image (a) has undergone a rotation angle of $\theta = 4^\circ$ and a translation vector $\vec{T} = (10pixels, 5pixels)$.

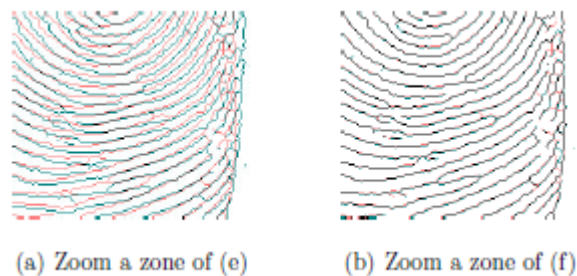


FIGURE 13: Zoom framed parts of the Ic (e) and (f).

On the second test, we show the results obtained by the proposed method in image of Figure 14. The Figure 14-(d), shows the result of the registration of the images in grayscale, while the Figure 14-(f) shows the result of the registration Ic extracted from the images in Figure 14-(a)-(b). Figure 15 shows the zoom of the framed images of Figure 14-(e) and 14-(f).

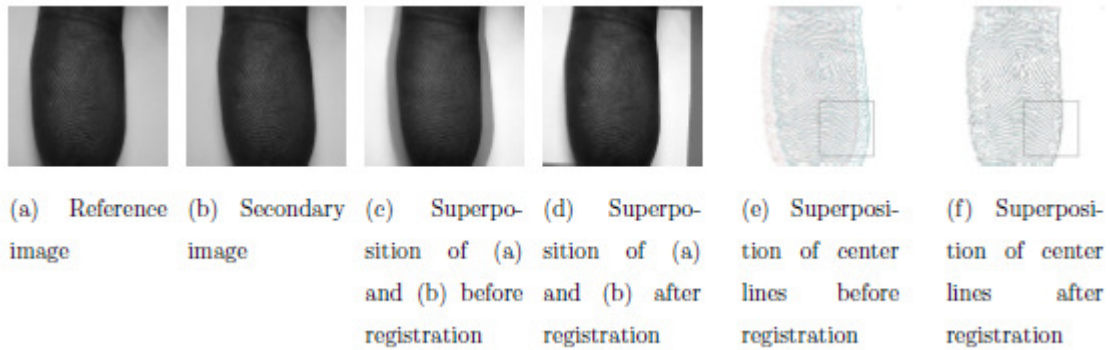


FIGURE 14: Result of registration. The images (a) and (b) are acquired at different times.

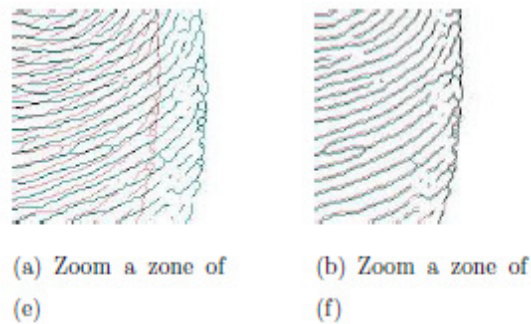


FIGURE 15: Zoom framed parts of the Ic (e) and (f).

The results in Table 4, show that on each interest point, landmark error is less than 1 pixel. The value of the RMSE calculated on the total 13 points is less than 0.5 pixel, which is relatively high precision.

Interest points	1	2	3	4	5	6	7	8
RMSE	0.5660	0.1608	0.4171	0.0270	0.0287	0.0020	0.36894	0.1985

Interest points	9	10	11	12	13	RMSE totale
RMSE	0.0593	0.0435	0.0965	0.0874	0.2004	0.4166

TABLE 2: Second test : The RMSEs calculated at interest points (in pixels).

We compared our method to that used descriptors Scale Invariant Feature Transform [35]. A plugin implements a registration method SIFT operator ImageJ was developed under the name of "SIFT Correspondences Extract" and "Extract MOPS Correspondences". We built this plugin to our platform to conduct experiments. The plugins "Extract SIFT Correspondences" and "Extract MOPS Correspondences" identify a set of corresponding points of interest in two images and export them as PointRoi. Interest points are detected using the Difference of Gaussian detector thus providing similarity-invariance [36]. Corresponding points are best matches from local feature descriptors that are consistent with respect to a common geometric transformation. The plugins use the Scale Invariant Feature Transform (SIFT) and Multi-Scale Oriented Patches (MOPS) for local feature description. The thus established matches are filtered using the RANSAC.

Figure 16 gives an illustration of the error curve for both methods with respect to the estimate of the rotation angle. The minimum error for both methods is 0 while the maximum error is 0.08 for our method and 0.043 for the method using SIFT.

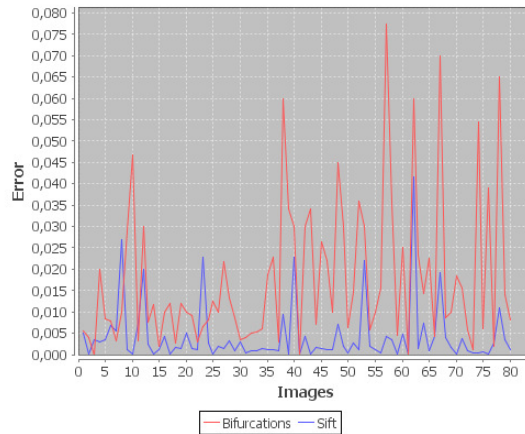


FIGURE 16: Relative error curves.

For the estimation of the translation vector, we have represented the module of real translation vectors and module of estimated translations vectors by each method. Figure 17 shows that the two modules regarding the real translations vectors and those estimated by our method are nearby. It may be noted at Figure 18 there is a very poor estimate of translation vectors by the method using SIFT.

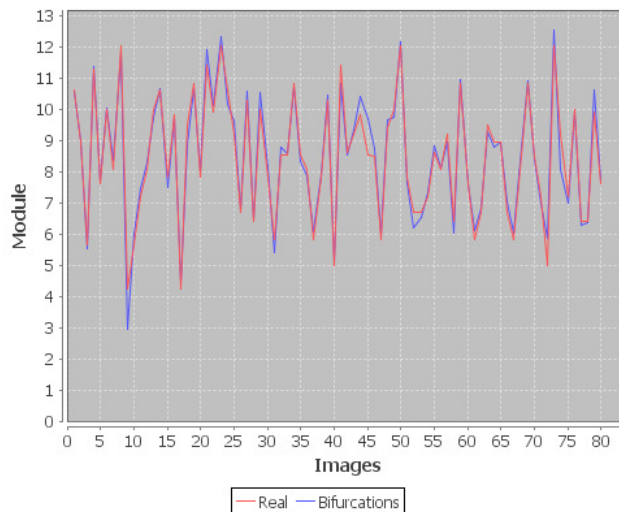


FIGURE 17: Module parameters real and estimated by bifurcations.

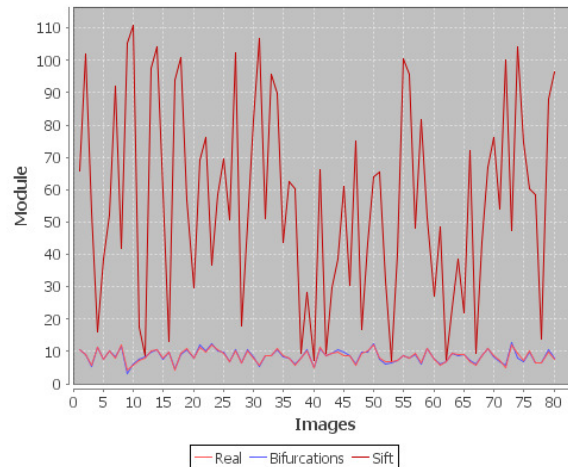


FIGURE 18: Module parameters real and estimated by bifurcations and SIFT.

5. CONCLUSION

In this paper, we have presented a new approach of the registration of fingerprint images that includes a segmentation technique to extract the streaks, a skeletonization technique to extract the center line streaks and a technique for extracting landmarks to guide the registration. The corresponding points, enabling the quantification of the deformation parameters existing between the images are obtained by comparing the correlation coefficients between the descriptor vectors of Zernike moments. The results obtained have allowed us to measure the reliability of the proposed method. The remaining work is about individuals identification using our registration method.

6. REFERENCES

- [1] S. Pankanti, S. Prabhakar, A. Jain, On the individuality of fingerprints, *IEEE Trans. Pattern Anal.* 24 (8) (2002) 1010–1025.
- [2] Biometric in governments post-9/11, National Science and Technology Council, <http://www.biometrics.gov/Documents/> (2009) 71–73, [Oct. 20, 2014].
- [3] B. Zitova, J. Flusser, Image registration methods: a survey, *Image and Vision Computing* 21 (2003) 977–1000.
- [4] L. Liu, T. Jiang, J. Yang, al, Fingerprint registration by maximization of mutual information, *IEEE Transactions on image processing* 15 (5) (2006) 1100–1110.
- [5] K. Mali, S. Bhattacharya, Fingerprint recognition using global and local structures, *International Journal on Computer Science and Engineering (IJCSE)* 3 (1) (2011) 161–172.
- [6] R. Bahuguna, Fingerprint verification using hologram matched filterings, *Psychological Review Presented at the 8th Meeting Biometric Consortium, San Jose, CA, Jun. 1996.*
- [7] S. Gold, A. Rangarajan, A graduated assignment algorithm for graph matching, *IEEE Trans. Pattern Anal.* 18 (4) (1996) 377–388.
- [8] D. K. Izenor, S. G. Zaky, Fingerprint identification using graph matching, *Pattern Recognit.* 19 (2) (1986) 113–122.
- [9] Y. He, J. Tian, X. Luo, T. Zhang, Image enhancement and minutiae matching in

- fingerprint verification, *Pattern Recognition Letters* 24 (2003) 1349–1360.
- [10] C. Serief, Robust feature points extraction for image registration based on the nonsubsampling contourlet transform., *International Journal of Electronics Communication*. 63 (2) (2009) 148–152.
- [11] J. Sarvaiya, S. Patnaik, H. Goklani, Image registration using nsct and invariant moment, *International Journal of Image Processing (IJIP)* 4 (2) (2010) 119–130.
- [12] G. Parziale, E.-D. Santana, R. Hauke, The surround imager: A multi-camera touchless device to acquire 3d rolled-equivalent fingerprints, *ICB, LNCS 3832* (2006) 244–250.
- [13] B. Hiew, A. Teoh, Y. Pang, Touch-less fingerprint recognition system, *ICB, LNCS 3832* (2007) 24–29.
- [14] S. Mil'shtein, J. Palma, C. Liessner, M. Baier, A. Pillai, A. Shendye, Line scanner for biometric applications, *IEEE Intern. Conf. on Technologies for Homeland Security* (2008) 205–208.
- [15] R. D. Labati, A. Genovese, V. Piuri, F. Scotti, Measurement of the principal singular point in contact and contactless fingerprint images by using computational intelligence techniques, *IEEE International Conference on Computational Intelligence for Measurement Systems and Applications (CIMS)* (2010) 18–23.
- [16] C. Lee, S. Lee, J. Kim, S. J. Kim, Preprocessing of a fingerprint image captured with a mobile camera, *ICB, LNCS 3832* (2006) 348–355.
- [17] T. Djara, M. K. Assogba, A. Naït-Ali, Caractérisation spatiale des empreintes de l'index en analyse biométrique, *Actes du CARL, Yamoussoukro* (2010) 501–508.
- [18] W. Osterburg, T. Parthasarathy, T. E. S. Raghavan, al, Developpement of a mathematical formula for the calculation of fingerprint probabilities based on individual characteristics, *Journal of the American Statistical Association* 72 (360) (1977) 772–778.
- [19] C. Arcelli, G. S. di Baja, A width-independent fast thinning algorithm, *IEEE Trans. Pattern Anal. Mach. Intell.* (1985) 463–474.
- [20] N. Galy, Etude d'un système complet de reconnaissance d'empreintes digitales pour un capteur microsysteme à balayage, *Institut National Polytechnique de Grenoble - INPG (Thèse)* (2005) 463–474.
- [21] R. J. Prokop, A. P. Reeves, A survey of moment-based techniques for unoccluded object representation and recognition, *Computer Vision, Graphics, and Image Processing. Graphical Models and Image Processing* 54 (5) (1992) 438–460.
- [22] R. Mukundan, K. R. Ramakrishnan, *Moment Functions in Images Analysis. Theory and Applications*, (1998), Ch. Zernike Moments, pp. 57–68.
- [23] R. Mukundan, K. R. Ramakrishnan, Fast computation of Legendre and Zernike moments, *Pattern Recognition* 28 (9) (1995) 1433–1442.
- [24] R. Mukundan, A contour integration method for the computation of zernike moments of a binary image, *National Conference on Research and Development in Computer Science and its Applications* (1997) 188–192.

- [25] W. Y. Kim, P. Yuan, A practical pattern recognition system for translation, scale, and rotation invariance, In Proceedings of the Conference on Computer Vision and Pattern Recognition, IEEE Computer Society Press (1994) 391–396.
- [26] L. V. Gool, T. Moons, D. Ungureanu, Affine/photometric invariants for planar intensity patterns, In Proceedings of the 4th European Conference on Computer Vision (1996) 642–651.
- [27] A. Khotanzad, Y. H. Hong, Invariant image recognition by zernike moments, IEEE Trans. Pattern Anal. Mach. Intell. 12 (5) (1990) 489–497.
- [28] P. A. Elsen, E. J. D. Pol, M. A. Viergever, Medical image matching a review with classification, IEEE Engineering in Medicine and Biology (1993) 26–39.
- [29] M. A. Fischler, R. C. Bolles, Random sample consensus: A paradigm for model fitting with applications to image analysis and automated cartography, Communications of the ACM, 24(6) (1981) 381–395.
- [30] T. Kim, W. Yu, Performance evaluation of ransac family, In Proceedings of the British Machine Vision Conference (BMVC). (2009) 1–12.
- [31] Q. Zhao, L. Zhang, D. Zhang, N. Luo, Direct pore matching for fingerprint recognition, M. Tistarelli and M.S. Nixon (Eds.), ICB (2009) 597–606.
- [32] F. Liu, Q. Zhao, L. Zhang, D. Zhang, Fingerprint pore matching based on sparse representation, Pattern Recognition (ICPR) (2010) 1630–1633.
- [33] R. Hartley, A. Zisserman, Multiple View Geometry in Computer Vision, 2nd Edition, (2004), Ch. Estimation - 2D Projective Transformations, pp. 117–121.
- [34] T. Svoboda, Ransac random sample consensus, <http://cmp.felk.cvut.cz> (2008) 1–18.
- [35] Lowe, David G. "Distinctive Image Features from Scale-Invariant Keypoints". *International Journal of Computer Vision* **60** (2): 91–110. (2004).. doi:10.1023/B:VISI.0000029664.99615.94.
- [36] Stephan Saalfeld. "Feature Extraction SIFT/MOPS (Fiji)". (2008). http://fiji.sc/Feature_Extraction

Robust Digital Image Watermarking Technique in DWT domain based on HVS and BPNN

B.Jagadeesh

Associate Professor
E.C.E.Department
G.V.P.College of Engineering (Autonomous)
Visakhapatnam, AP, India.

bjagadeesh76@yahoo.com

P.Rajesh Kumar

Professor, E.C.E.Department
Andhra University
Visakhapatnam, AP, India.

rajeshauce@gmail.com

P.Chenna Reddy

Professor, C.S.E.Department
JNTUA College of Engineering, Pulivendula
Kadapa, AP, India.

pcreddy1@rediffmail.com

Abstract

Most of the data distribution or redistribution occurs on the internet either by means of images, documents, videos, etc. But to claim the ownership and copy right protection, some extra information which cannot be removed by intruders is necessary to provide security. Such a security is provided by Watermarking. In this paper, a robust Digital Image watermarking algorithm is projected in Discrete Wavelet Transform domain using back propagation neural networks and Human Visual System Parameters like Luminous sensitivity and Texture sensitivity. Neural Networks are used in embedding and extracting the watermark. The proposed method is more protected and robust to several attacks like: Resizing, Median filtering, Row-Column copying, Low pass filtering, JPEG Compression, Rotation, Salt and Pepper Noise, Cropping, Bit Plane Removal, Blurring, Row-Column blanking, Intensity Transformation, etc. Outstanding experimental outcomes were perceived with the suggested method over a method proposed by Qiao Baoming et al. in terms of Peak Signal to Noise Ratio (PSNR) and Normalized Cross Correlation (NCC).

Keywords: Image Watermarking, Discrete Wavelet Transform, Human Visual System, Back Propagation Neural Networks, Imperceptible, Robust.

1. INTRODUCTION

With the greatest advancement in technology and usage of internet, lossless copying and powerful tools for editing have been emerged. In such a scenario, it is quite necessary to claim the ownership. Digital Image Watermarking is one of the best methods for copyright protection [1,2]. It is a technique in which some secret information called watermark data is embedded in the original image or host image. Then, the watermarked image is detected for watermark for illegal copying, ownership protection etc. [3]. Digital Watermarking provides two basic requirements as robustness and perceptual transparency [4]. The term robustness indicates flexibility of inserted watermark in contrast to distortions and attacks that try to remove the embedded watermark. Perceptual transparency indicates that watermark embedding must not lower the quality of watermarked data [5]. According to watermarking domain, watermarking methods can be classified into spatial domain methods [6] & transform domain methods [7-10].

In order to increase imperceptibility of watermarked image and robustness of watermark, many scholars have made various research based on Neural Network Techniques [11-20].

Asmaa Qasim Shareef et al. [11] suggested a watermarking algorithm based on back propagation based learning algorithm and feed-forward multi-layered neural network. Back-propagation centered learning algorithm is used to get the weights and these weights are inserted within the original cover image, which was processed from noise by the Gaussian filter. Maryam Karimi et al. [12] described a transparent image signal watermarking method centered on psychovisual properties using Multi-Layer Feed-forward (MLF) neural networks. The blocks which are less detectable by human eye are identified by using MLF neural networks and they are used for embedding the watermark. Mohamad Vafaei et al. [13] projected a method based on wavelet coefficient quantization using artificial neural networks. A digital watermarking algorithm based on feed-forward neural networks was presented. Sameh Oueslati et al. [14] suggested an adaptive image signal watermarking method centered on the Human Visual System (HVS) model and neural network method. This method uses Back Propagation Neural Network for embedding the watermark. HVS parameters are fed to neural network as input and target vectors.

N. Mohananthini et al. [15] presented a digital image signal watermarking method centered on Back-Propagation Neural Networks (BPNN) & Human Visual System. Using improved BPNN, watermark image is embedded into Discrete Wavelet Transform (DWT), which can reduce the error and improve the rate of the learning; trained neural networks are used to rebuild the watermark image signal from the watermarked image. Qiao Baoming et al. [16] projected a watermarking method centered on Back Propagation Neural Network (BPNN) and Discrete Wavelet Transform (DWT). 2-level DWT is applied to host cover image. Blocks are selected based on standard deviation values. Block values are fed to network as input and target vectors.

Yonghong Chen et al. [17] proposed an image watermarking scheme combining backpropagation neural network, error correction coding and chaotic sequence in wavelet transform domain. The wavelet transform domain of cover image is first divided into set of blocks, and later different back propagation neural network simulations for every selected block are exercised to remember relationship between samples and equivalent sub sequence is separated from a processed disordered sequence. The watermark image is embedded by varying a small number of wavelet transform coefficients. Song Huang et al. [18] projected an image watermarking scheme based on Image features, fractional dimension technique to form the watermark and back propagation neural networks. The watermark used is fusion of a binary image and image feature label and obtained by investigating the image fractal dimension. This watermark is scrambled by using Arnold transform and inserted into the multi wavelet transformed cover image. Back propagation neural network was applied to increase the transparency and robustness.

This paper is a modified watermarking method using Human Visual System parameters for inserting the watermark image established on scheme projected by Qiao Baoming et al. [16] in which, coefficients of 3x3 non overlapping blocks are chosen as inputs to neural networks. But the Proposed method makes use of HVS parameters like Luminous and Texture sensitivity values as inputs which gives better imperceptibility and robustness.

The rest of the document is planned as follows: Section 2 illustrates Preliminaries about Discrete Wavelet Transform & Back Propagation Neural Network. Section 3 describes the suggested watermarking scheme. Experimental results are presented in section 4. Conclusions are specified in section 5.

2. PRELIMINARIES

2.1 Discrete Wavelet Transformation (DWT)

DWT is most suitable for transient, time varying signals because the wavelets obtained after DWT have their energy focused in time and most of the real life signals vary with time; hence DWT is presently applied in wide range of signal processing usages such as in video & audio

compression, elimination of noise in audio etc. The elementary thought of Discrete Wavelet Transform in image processing is to decay the image into sub image of dissimilar spatial domains & independent frequencies. After DWT transformation, four wavelets as (LL, LH, HL, HH) bands are obtained. This is single level or 1-level DWT. The low-frequency wavelet data can be again decayed into sublevel frequency wavelet data of LL2, HL2, LH2 and HH2 respectively. Similarly any wavelet can be further decomposed. In this paper, HH band is further decomposed into three sub levels as shown in Figure 1. So, the host image can be disintegrated for n level wavelet conversion.

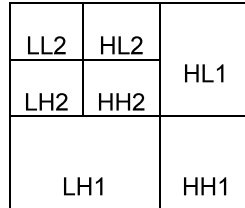


FIGURE 1: DWT Wavelets after Transformation.

2.2 Back Propagation Neural Network (BPNN)

BPNN is one of the artificial neural network. The Artificial Neural Network is a data handling system with features called neurons to process the information content. The signals are spread by ways of the connection links with accompanying weight that is multiplied with arriving signal to obtain the net input for any typical neural network. The output signal is acquired by employing activation to the net input. Back Propagation provides an efficient method for changing weights by back propagation of errors in a feed forward network. Figure 2 shows back propagation neural network.

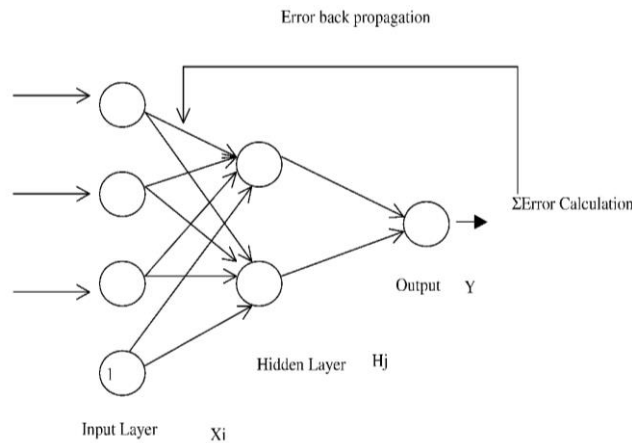


FIGURE 2: Back Propagation Neural Network.

In this network the total squared error of output is reduced by gradient descent method acknowledged as back propagation or generalized delta rule. The increase in number of hidden layers result in the computational difficulty of network and hence time taken to reduce the error may be very high.

The back propagation training algorithm has four stages:

1. Initializing the weights
2. Feed forwarding
3. Back propagating the errors
4. Updating the biases and weights

The bias acts like weights on the linking from units whose output is always 1. During initialization of weights, some arbitrary values are given initially to give some output by feed forwarding through the layers. So, the difference between the obtained and actual values is calculated as error and back propagated. High initial weight will result in fast learning rate. But weights may oscillate. If initial weights are too small, then learning rate will be slow. For best results, initial weights may be considered between -0.5 to 0.5 or -1 to 1.

3. THE PROPOSED METHOD

The proposed scheme involves watermark insertion & extraction schemes which are given below:

3.1 Watermark Embedding

1. The host image is a gray level image of dimension 512x512 pixels.
2. The binary image of dimension 32x32 pixels is chosen as watermark.
3. One level DWT is employed on host image and cD1 is split into 3x3 non-overlapping blocks.
4. 1024 blocks are selected based on their standard deviation values (in ascending order).
5. The selected block numbers is provided as secret key1 that is used for extraction of watermark.
6. HVS parameters like Luminance and Texture sensitivity are calculated for the selected 1024 blocks.
7. These are fed as input to neural network and centre element of each block as target vector.
8. Centre element from each block is chosen for embedding watermark.
9. Embedding formula is as follows

$$C' = C + (2 * \alpha + 1) * (2 * (w_{ok}) - 1) \quad (1)$$

Where α is adaptive weight of watermark (BPNN output), C is center coefficient and w_{ok} is watermark bit.

10. One level IDWT is employed to obtain the watermarked image.

3.2 Watermark Extraction

1. 1-level DWT is applied to watermarked image and cD1 is divided into 3x3 non-overlapping blocks.
2. Based on the key1, 1024 blocks are selected.
3. For the selected blocks, Centre value in each block is provided to BPNN as target vector, and HVS parameters like Luminance and Texture sensitivity of selected 1024 blocks are fed as input vector.
4. By using some additional information and BPNN output, watermark can be extracted by using reverse embedding equation.

$$\text{Extracted watermark} = (\text{emb} - \text{obt}) / (4 * y_1 + 2) + 0.5 \quad (2)$$

Where 'emb' is matrix of 1024 elements after embedding, 'obt' is obtained 1024 elements matrix during extraction and y_1 is output from neural network.

The Peak Signal to Noise Ratio (PSNR) and Normalized Cross correlation (NCC) are exploited to test the working of the proposed algorithm. Let us consider the cover image signal of size $M \times M$ be denoted as $g(i,j)$ and let the watermarked signal equivalent be $G(i,j)$. Then the PSNR is known by

$$\text{PSNR} = 10 \log_{10} \left(\frac{\sum_{i=1}^M \sum_{j=1}^M (g(i,j))^2}{\sum_{i=1}^M \sum_{j=1}^M (g(i,j) - G(i,j))^2} \right) \quad (3)$$

Watermark signal is symbolized by $w_m(i,j)$ & let recovered watermark signal be symbolized by $w'_m(i,j)$, then the NCC is given as

$$NCC = \frac{\sum_{i=1}^M \sum_{j=1}^M (wm(i,j) - wmean)(w'm(i,j) - w'mean)}{\sqrt{\sum_{i=1}^M \sum_{j=1}^M (wm(i,j) - wmean)^2 \sum_{i=1}^M \sum_{j=1}^M (w'm(i,j) - w'mean)^2}} \quad (4)$$

In Eq. (4), Wmean & W'mean specify the average of the unique watermark and removed watermark signals correspondingly.

4. EXPERIMENTAL RESULTS

Experimentations are conducted to assess the performing of the algorithm using cover gray-scale images 'LENA', 'PEPPERS' and 'MANDRILL' which are shown in Figure 3.

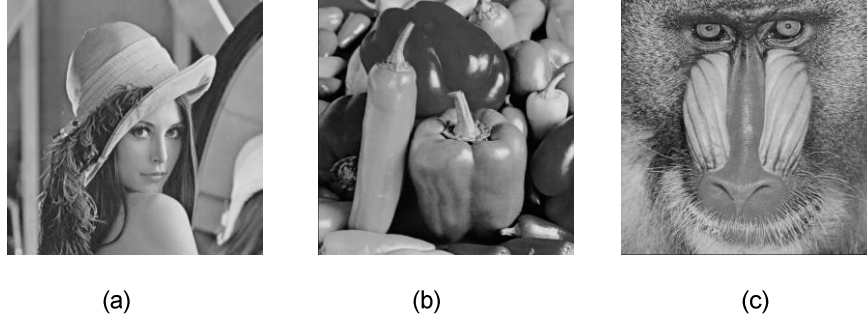


FIGURE 3: 512x512 (a) Lena, (b) Peppers and (c) Mandrill (Host Images).

The host images are of sizes 512 x 512 pixels. The size of watermark image signal of 32 x 32 pixels is a logo represented with the letters 'ECE' as shown in figure 4.



FIGURE 4: Watermark Image.

In Figure 5 Watermarked Lena, Peppers and Mandrill are shown.

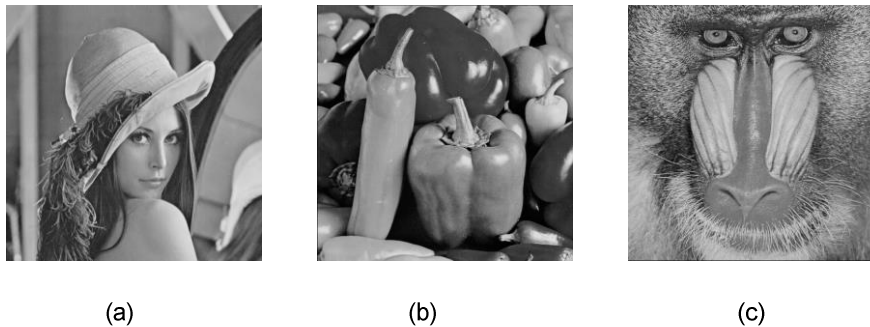


FIGURE 5: 512x512 Watermarked (a) Lena (47.69dB), (b) Peppers (45.78dB) and Mandrill (37.25dB).

Different attacks that are exploited to assess the robustness of the watermarked image signal are Low pass filtering, Resizing, Row-Column copying, Rotation, JPEG Compression, Salt and Pepper Noise, Cropping, Median filtering, Gamma correction, Bit Plane Removal, Blurring, Row-Column blanking, Histogram equalization, Intensity Transformation. All these attacks were experimented using MATLAB 7.8.0. Peak Signal to Noise Ratio (PSNR) and Normalized Cross correlation (NCC) are exploited as the performance metric to evaluate the transparency and robustness and are synopsisized in Tables 1, 2 and 3. Extracted watermark images from the watermarked images are shown in Table 4.

Type of Attack	Qiao Baoming et al. [16] method		Proposed method	
	PSNR in dB	NCC	PSNR in dB	NCC
No attack	47.73	0.9742	47.69	0.9995
Median Filtering	41.04	0.4998	41.16	0.8884
Resize (512-256-512)	40.07	0.5206	40.12	0.9239
Row-Column blanking	31.47	0.0524	31.47	0.9453
Row-Column copying	38.10	0.1744	38.10	0.8426
Rotation	37.15	0.5579	28.01	0.9017
JPEG Compression (QF:90)	44.27	0.6350	45.08	0.8821
Low pass Filtering (3x3 Kernel)	37.87	0.1248	37.95	0.9244
Salt & Pepper Noise(0.001)	40.96	0.3554	40.46	0.9846
Cropping	18.48	0.0070	18.48	0.9661
Gamma Correction(0.9)	19.27	0.8167	19.28	0.9492
Bit plane removal	46.09	0.7258	46.17	0.8971
Histogram Equalization	25.14	0.4388	25.12	0.8436
Blurring	41.16	0.6299	41.37	0.9222
Intensity Transformation	28.05	0.7404	28.06	0.9466

TABLE 1: Comparison of PSNR and NCC values for Lena image with Qiao Baoming et al. [16] scheme and the proposed method.











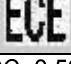




Type of Attack	Qiao Baoming et al.[16] method		Proposed method	
	PSNR in dB	NCC	PSNR in dB	NCC
No attack	43.13	0.9822	45.78	0.9984
Median Filtering	39.96	0.3930	40.90	0.8657
Resize (512-256-512)	37.92	0.4308	38.01	0.9113
Row-Column blanking	32.28	0.0998	32.44	0.5953
Row-Column copying	36.71	0.1998	37.15	0.5579
Rotation	27.69	0.1559	27.73	0.8919
JPEG Compression (QF:90)	41.08	0.6007	43.54	0.8002
Low pass Filtering (3x3 Kernel)	37.38	0.1759	37.62	0.9096
Salt & Pepper Noise(0.001)	39.23	0.2636	39.53	0.9775
Cropping	17.81	0.0960	17.81	0.9579
Gamma Correction(0.9)	19.94	0.6274	19.97	0.9242
Bit plane removal	42.57	0.7474	44.76	0.8718
Histogram Equalization	24.59	0.3889	24.60	0.7370
Blurring	39.21	0.5043	39.91	0.8751

Intensity Transformation	27.37	0.8178	27.38	0.9539
--------------------------	-------	--------	-------	--------

TABLE 2: Comparison of PSNR and NCC values for Peppers image with Qiao Baoming et al. [16] scheme and the proposed method.

Type of Attack	Qiao Baoming et al. [16] method		Proposed method	
	PSNR in dB	NCC	PSNR in dB	NCC
No attack	34.39	0.9714	37.25	0.9928
Median Filtering	29.34	0.0968	29.77	0.8512
Resize (512-256-512)	29.59	0.0527	29.67	0.8360
Row-Column blanking	28.96	0.0274	29.59	0.3334
Row-Column copying	32.81	0.4406	34.56	0.9424
Rotation	26.99	0.1472	27.26	0.8845
JPEG Compression (QF:90)	33.86	0.5242	36.37	0.6996
Low pass Filtering (3x3 Kernel)	29.06	0.0750	29.30	0.7753
Salt & Pepper Noise(0.001)	33.68	0.3421	36.02	0.9905
Cropping	17.79	0.1499	17.81	0.9634
Gamma Correction(0.9)	18.89	0.2963	18.95	0.9467
Bit plane removal	34.32	0.7733	37.08	0.9269
Histogram Equalization	23.11	0.1582	23.35	0.8069
Blurring	30.42	0.1066	31.02	0.8502
Intensity Transformation	25.21	0.2377	25.58	0.9300

TABLE 3: Comparison of PSNR and NCC values for Mandrill image with Qiao Baoming et al. [16] scheme and the proposed method.

Type of attack	Watermarked image Type		
	Lena	Peppers	Mandrill
No attack			
	NCC: 0.9995	NCC:0.9984	NCC:0.9928
Median Filtering			
	NCC: 0.8884	NCC: 0.8657	NCC: 0.8512
Resize (512-256-512)			
	NCC: 0.9239	NCC: 0.9113	NCC: 0.8360
Row-Column blanking			
	NCC: 0.9453	NCC: 0.5953	NCC: 0.3334
Row-Column copying			
	NCC: 0.8426	NCC: 0.5579	NCC: 0.9424

























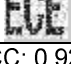
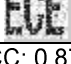

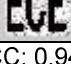

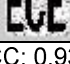
Rotation			
	NCC: 0.9017	NCC: 0.8919	NCC: 0.8845
JPEG Compression (QF:90)			
	NCC: 0.8821	NCC: 0.8002	NCC: 0.6996
Low pass Filtering (3x3 Kernel)			
	NCC: 0.9244	NCC: 0.9096	NCC: 0.7753
Salt & Pepper Noise(0.001)			
	NCC: 0.9846	NCC: 0.9775	NCC: 0.9905
Cropping			
	NCC: 0.9661	NCC: 0.9579	NCC: 0.9634
Gamma Correction(0.9)			
	NCC: 0.9492	NCC: 0.9242	NCC: 0.9467
Bit plane removal			
	NCC: 0.8971	NCC: 0.8718	NCC: 0.9269
Histogram Equalization			
	NCC: 0.8436	NCC: 0.7370	NCC: 0.8069
Blurring			
	NCC: 0.9222	NCC: 0.8751	NCC: 0.8502
Intensity Transformation			
	NCC: 0.9466	NCC: 0.9539	NCC: 0.9300

TABLE 4: Extracted Watermarks from the watermarked image.

The bar plot in Figure 6 shows the PSNR values for proposed method and Qiao Baoming et al. [16] algorithm.

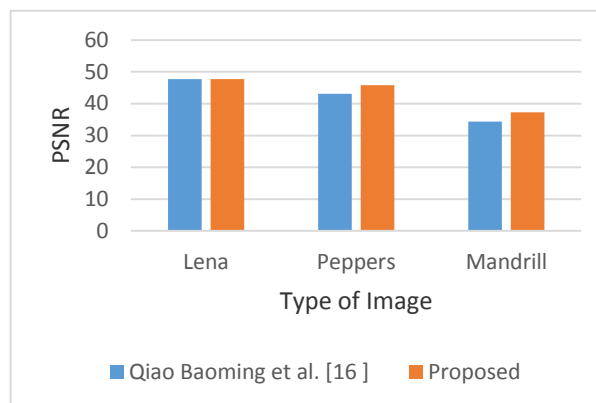


FIGURE 6: PSNR Values of watermarked test images.

The plots in Figures 7, 8 and 9 displays the NCC values for the extracted watermark from test images when image processing attacks are applied to it along with the NCC values from Qiao Baoming et al. [16].

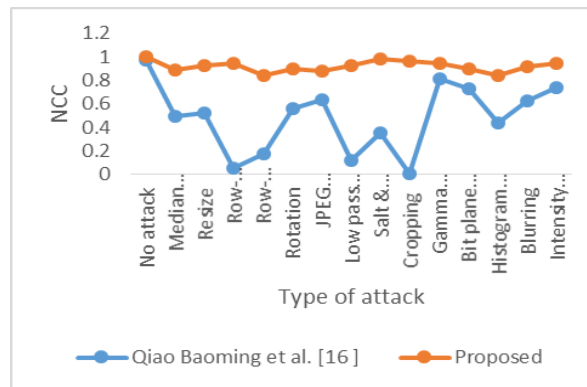


FIGURE 7: NCC values of the extracted watermark under various attacks from the watermarked Lena image.

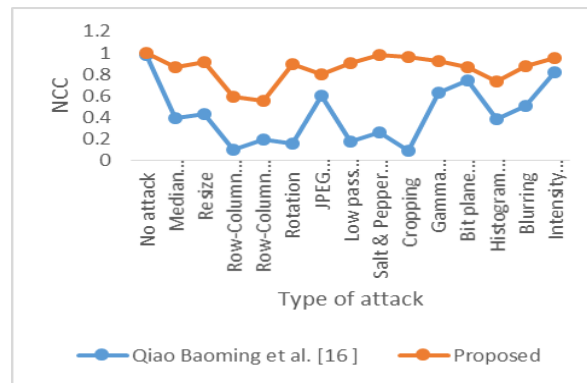


FIGURE 8: NCC values of the extracted watermark under various attacks from the watermarked Peppers image.

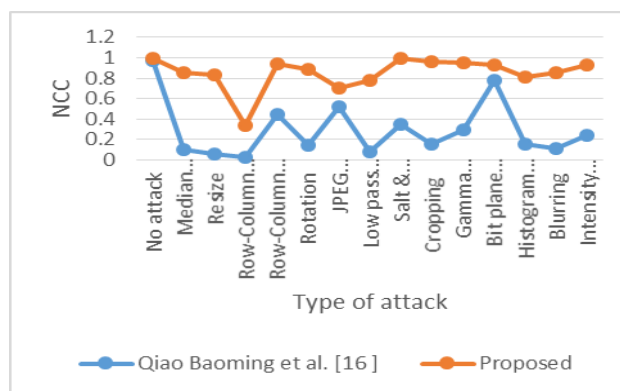


FIGURE 9: NCC values of the extracted watermark under various attacks from the watermarked Mandrill image.

5. CONCLUSIONS

In this paper, an algorithm centered on Discrete Wavelet Transform and Back Propagation Neural Network using Human Visual System parameters like Luminous sensitivity and Texture sensitivity has been presented. HVS parameters usage as inputs to the neural network and DWT gives better performance as compared to neighboring coefficients as inputs as in Qiao Baoming et al. [16] method. The projected algorithm is extremely robust and sustained many image processing attacks. Using other Artificial Intelligence techniques like Fuzzy and Hybrid Intelligence Techniques, robustness and imperceptibility can be improved.

6. REFERENCES

- [1] Cox, IJ, Miller, ML & Bloom, JA. Digital Watermarking. San Francisco, CA, USA: Morgan Kaufmann Publisher, 2002.
- [2] Fotopoulos V., and Skodras A.N. " Digital image watermarking: An overview", invited paper, EURASIP Newsletter, ISSN 1687-1421, Vol. 14, No. 4, pp. 10-19, 2003.
- [3] F. H. Wang, J. S. Pan, and L. C. Jain. "Digital Watermarking Techniques", In Innovations in Digital Watermarking Techniques, Berlin, Heidelberg: Springer-Verlag, pp. 11-26, 2009.
- [4] Chin-Chen Chang, Yih-Shin Hu, Tzu-Chuen Lu. "A watermarking-based image ownership and tampering authentication scheme", Pattern Recognition Letters, pp. 439-446, (27), 2006.
- [5] C.I.Podilchuk and E.J.Delp. "Digital Watermarking: Algorithms and Applications", IEEE Signal Processing Magazine, pp.33-46, July 2001.
- [6] N Nikolaidis, I Pitas. "Robust image watermarking in the spatial domain", Signal Process. 66 (3); pp.385-403, 1998.
- [7] W.C.Chu. "DCT based image watermarking using sub sampling," IEEE Trans Multimedia 5, 34-38, 2003.
- [8] Y. Wang, R.E.Van Dyck and J.F.Doherty. "A wavelet based watermarking algorithm for ownership verification of digital images", IEEE Transactions on Image Processing, Volume 11, No.2, pp.77-88, February 2002.
- [9] Nader H. H. Aldeeb, Ibrahim S. I. Abuhaiba. "An Improved Watermarking Scheme for Tiny Tamper Detection of Color Images", I.J. Image, Graphics and Signal Processing, 5, pp. 1-14, 2013.
- [10] R.Liu, T.Tan. "An SVD-based watermarking scheme for protecting rightful ownership", IEEE Transactions on Multimedia, vol.4, no.1, pp. 121-128, 2002.
- [11] Asmaa Qasim Shareef, and Roaa Essam Fadel. "An Approach of an Image Watermarking Scheme using Neural Network" International Journal of Computer Applications, Volume 92 – No.1, pp. 44-48, April 2014.
- [12] Maryam Karimi, Majid M., Azizi S., and Samavi S. "Transparent watermarking based on psychovisual properties using neural networks", Proceedings of the Iranian Conference on Machine Vision and Image Processing (MVIP), Zanjan, September, 2013, pp. 33-37.
- [13] Mohamad Vafaei, Homayoun, and Mahdavi-Nasab. "A Novel Digital Watermarking Scheme Using Neural Networks with Tamper Detection Capability", Journal of Basic and Applied Scientific Research, Vol. 3(4), pp. 577-587, 2013.
- [14] Sameh Oueslati, Adnene Cherif, and Bassel Solaimane. "Adaptive Image Watermarking Scheme Based on Neural Network", International Journal of Engineering Science and Technology (IJEST), Vol. 3, No. 1, January, pp. 748-756, 2011.

- [15] N. Mohananthini, and G. Yamuna. "Watermarking for Images using Wavelet Domain in Backpropagation Neural Network", Proceedings of the IEEE -International Conference on Advances in Engineering, Science and Management (ICAESM -2012), Nagapatnam, Tamil Nadu, March 2012, pp. 100-105.
- [16] Qiao Baoming, Zhang Pulin, and Kang Qiao. "A Digital Watermarking Algorithm Based on Wavelet Packet Transform and BP Neural Network", Proceedings of the IEEE International Conference on Computational Intelligence and Security, Hainan, 2011, pp. 503-507.
- [17] Yonghong Chen, and Jiancong Chen. "A Novel Blind Watermarking Scheme Based on Neural Networks for Image", Proceedings of the IEEE International Conference on Information Theory and Information Security (ICITIS), Beijing, 2010, pp. 548-552.
- [18] Song Huang, and Wei Zhang. "Digital Watermarking Based on Neural Network and Image Features", Proceedings of the IEEE Second International Conference on Information and Computing Science, Manchester, 2009, pp. 238-240.
- [19] Song Huang, Wei Zhang, Wei Feng, and Huaqian Yang, "Blind Watermarking Scheme Based on Neural Network", Proceedings of the 7th World Congress on Intelligent Control and Automation, Chongqing, China, June, 2008, pp.5985-5989.
- [20] Xuelong Hu, Xu Lian, Lin Chen, and Yongai Zheng, "Robust Blind Watermark Algorithm of Color Image Based on Neural Network", Proceedings of the IEEE International Conference Neural Networks & Signal Processing, Zhenjiang, China, June, 2008, pp.430-433.

Hybrid Domain based Face Recognition using DWT, FFT and Compressed CLBP

Sujatha B M

Dept. of ECE,
Acharya Institute of Technology,
Bangalore, India.

sujaathabm2005@gmail.com

K Suresh Babu

Dept. of ECE,
University Visvesvaraya College of Engineering,
Bangalore, India.

Ksb1559@gmail.com

K B Raja

Dept. of ECE,
University Visvesvaraya College of Engineering,
Bangalore, India

raja_kb@yahoo.com

Venugopal K R

University Visvesvaraya College of Engineering
Bangalore, India.

venugopalkr@gmail.com

Abstract

The characteristics of human body parts and behaviour are measured with biometrics, which are used to authenticate a person. In this paper, we propose Hybrid Domain based Face Recognition using DWT, FFT and Compressed CLBP. The face images are preprocessed to enhance sharpness of images using Discrete Wavelet Transform (DWT) and Laplacian filter. The Compound Local Binary Pattern (CLBP) is applied on sharpened preprocessed face image to compute magnitude and sign components. The histogram is applied on CLBP components to compress number of features. The Fast Fourier Transformation (FFT) is applied on preprocessed image and compute magnitudes. The histogram features and FFT magnitude features are fused to generate final feature. The Euclidian Distance (ED) is used to compare final features of test face images with data base face images to compute performance parameters. It is observed that the percentage recognition rate is high in the case of proposed algorithm compared to existing algorithms.

Keywords: Biometrics, CLBP, DWT, Face Recognition, FFT, Histogram.

1. INTRODUCTION

The biometrics stands for life measurements i.e., the measurement and analysis of biological characteristics such as fingerprints, iris patterns, retina etc. or the behavioural characteristics such voice, gait, signature etc. of an individual. The identification of a person is based on biological factors and behavioural characteristics. Some of the different types of biological biometrics are: (i) *Fingerprint Recognition*: The ridges and valleys in the fingertips to identify an individual. The drawback with this approach is that most often it is possible for an individual to lose the fingerprints due to injury or due to working in hazardous work environments. (ii) *Face Recognition*: The facial characteristics of an individual are analysed. (iii) *Finger/Hand Geometry Recognition*: The special and transform domain features are analysed for recognition. (iv) *Iris Recognition*: An individual is identified based on the unique patterns of the iris. (v) *Retina Recognition*: Analysing the features of the capillary vessels present at the back of the eye. (vi) *Vein Detection*: The vein patterns in the back of the hand and the wrist is used to identify an

individual. The analysis of various behavioural characteristics to identify an individual are: (i) *Voice Recognition*: Analysing the tone, frequency and pitch of an individual's voice. (ii) *Signature Recognition*: Analysis of the style in which a person does the signature. (iii) *Keystroke Recognition*: Studying the pattern in which an individual types on the keyboard.

Face recognition is the biometric technique of identifying through the analysis of facial features. The key advantage of face recognition is that it does not require any cooperation from the subject under test. Most face recognition systems implemented in surveillance applications captures and analyses the individuals even without their knowledge. Face recognition has extensive application in both one-to-one mapping for verification of a person and one-to-many mapping for identification of an individual. One of the ways to achieve this is by first acquiring the facial features and then comparing it with the facial databases. The advantages and applications of face recognition is a hot field of research and challenging task for efficient identification under illuminations pose variations etc.

Contribution: In this paper Hybrid Domain based Face Recognition using DWT, FFT and Compressed CLBP is proposed. The Face images are preprocessed to sharpen the images. The CLBP is applied on face images to generate CLBP features. The histogram is applied to compress CLBP features. The FFT is applied on preprocessed image to generate magnitude features, which are fused with Histogram features to generate final features. The final test features and data base features are compared using ED.

Organisation: section 1 gives brief introduction of biometrics. The related work of existing techniques described in section 2. The proposed model is described in section 3. In section 4 algorithm is given. The performance analysis is discussed in section 5. The conclusion is given in section 6.

2. RELATED WORK

Faisal R.Al-Osaimi et al., [1] proposed a spatially optimised data/pixel-level fusion of 3D shape and texture. Here in order to make the expression and illumination variations reside better in PCA subspace, the fusion is spatially optimised with respect to multimodal pixel values. Also they proved that identification performance was further improved by using higher order fusion functions and multiple fusion functions systematically. Raghuraman Gopalan et al., [2] created a subspace resulting from convolution of an image with a set of orthogonal basis functions and showed that subspace created by clear image and its blurred versions are equal under ideal conditions of zero noise. Ping-Han Lee et al., [3] explored the orientations of edges and proposed Oriented Local Histogram Equalization (OLHE) which compensates illumination. The OLHE feature combinations schemes are used for viz, encoded most edge orientations, compactness with good edge-preserving capabilities and performs better in extreme lighting conditions. Discriminant nonlinear with Generalise Discriminant Analysis (GDA) was applied to LBP, Gabor and Local TernityPatterns (LTP) are used for feature extraction. Cosine distance based nearest neighbour is used for classification.

Timo Ahonen et al.,[4] proposed face recognition using Local Binary Pattern (LBP).The LBP features are extracted by dividing face into several regions and enhanced feature vectors are used for face recognition. In the field of 3D face recognition system. Parama Bagchi et al., [5] have given a robust system which can handle pose as well as occlusions. The system takes in 3D image, registers facial surfaces to common model minimizing distance between a probe model and gallery model using ICP (Iterative Closest Point) algorithm. Later the occlusions are extracted by thresholding depth map values of 3D image. The Principal Component Analysis (PCA) is used for feature extraction. Classification on the extracted features was performed using Artificial Neural Networks. Michel F.Valstar and Maja Pantic [6] have proposed a method for detecting larger facial behaviour by recognizing facial muscle actions that have expressions .The geometric features are used for recognition. The Support Vector Machine (SVMs) and Hidden Morkove Model (HMMs) are used for feature classification.

Wilman W.W.Zou and Pong C. Yuen [7] proposed a method to learn relation between the high resolution image spaces, very low resolution image (VRL) space and face super resolution (SR). Based on this new data and discriminative constraints were designed for good visibility. SVM and INN methods are used for classification. Hu Han et al., [8] have presented a generic frame work for automatic demographic (age, gender and race) estimation for a face image. Demographic informative features are extracted from biologically inspired features and they have predicted the demographic attributes of a face image using a hierarchical classifier to predict the age, gender and race. Changxing Ding et al., [9] proposed face identification for handling the full range of pose. First the original pose-invariant face recognition problem is transformed into a partial frontal face recognition problem. To represent the synthesised partial frontal faces, a robust patch based face representation scheme is developed.

Faisal Ahmed et al., [10] introduced a face recognition method using Compound Local Binary Pattern (CLBP). This method uses encoding scheme which combines magnitude information of the difference between two grey values along with original LBP pattern. The performance of CLBP features are classified using Support Vector Machines (SVM) classifier. Gae Yong Choi et al., [11] proposed colour texture features based on Colour Local Gabor Wavelets (CLGWs) and Colour Local Binary Pattern (CLBP) for face recognition. To perform classification multiple colour local textures are combined at the feature level with uniform weights.

3. PROPOSED MODEL

The block diagram of proposed model is shown in Figure1. The face images are pre-processed using DWT, Laplacian filtering and subtraction for better performance.

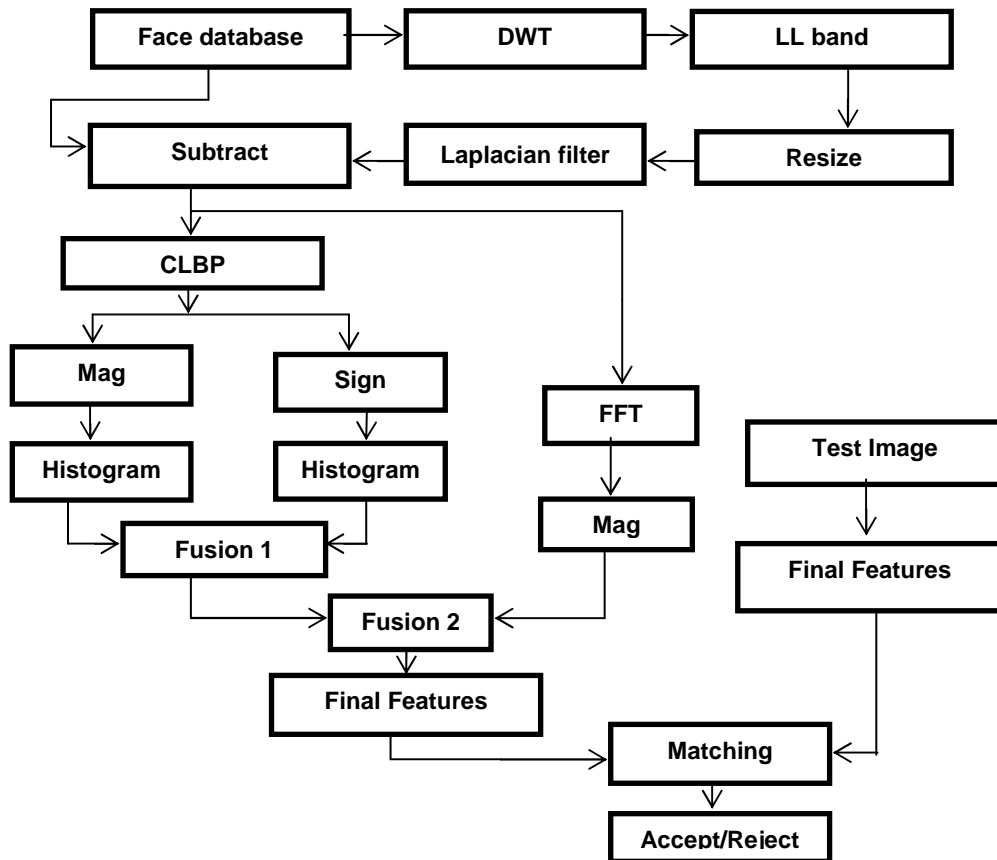


FIGURE 1: Block diagram of proposed model.

3.1 Face Database

The standard face databases such as JAFFE, ORL, Indian male and Indian female are considered to test the proposed model.

3.1.1 JAFFE Database

The JAFFE face data base [12] has 10 persons with approximately twenty face images per person. The different images captured for single person are based on facial expressions, such as emotional, happy, angry, disgust, surprise and neutral movements. The original size of image is 256x256 and ten image samples of a person are shown in Figure 2. For experimental results the data base is created by considering eight persons with seven images per person that is fifty six images to compute performance parameters FRR and TSR. The remaining two persons with one image per person are considered to compute FAR.



FIGURE 2: Samples of JAFFE face images of person.

3.1.2 ORL Database

The ORL database [13] shown in Figure 3 has forty persons with ten images per person. The ten different images of a same person are taken at different times by varying lightning, facial expression (which includes opening/closing of eyes and smiling/not smiling), facial details (glass/no glass).The database is created by considering first thirty persons out of forty persons and first six images per person are considered to create database which leads to one eighty images in the database and ninth image from first thirty persons are taken as test image to compute FRR and TSR. The remaining ten persons out of forty are considered as out of database to compute FAR.

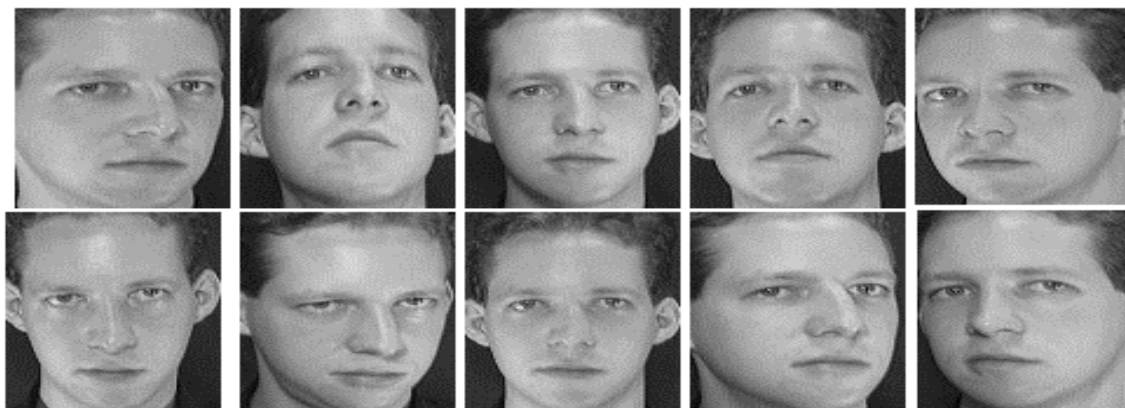


FIGURE 3: Samples of ORL face images of person.

3.1.3 Indian Male

The Indian male face database [14] shown in Figure 4 has twenty persons with approximately eleven images per person. The images were taken in homogeneous background with an upright and frontal position. The eleven different images include facial orientations such as looking front, looking left, looking right, looking up, looking up towards left, looking up towards right, looking down, with emotions neutral, smile, laughter, sad/disgust. The database is created by considering first twelve persons out of twenty persons with first six images per persons are considered to create database which leads to seventy two images in the database and ninth image from first twelve persons are taken as test image to compute FRR and TSR. The remaining eight persons out of twenty persons are considered as out of database to compute FAR.



FIGURE 4: Samples of Indian male data base face images

3.1.4 Indian Female

The Indian females face database [14] shown in Figure 5 consists of twenty two persons with approximately eleven images per person. The variations in pose and expressions are same as Indian male face database. The database is created by considering first fifteen persons out of twenty two persons with first seven images per persons are considered to create database which leads to hundred five images in the database and ninth image from first fifteen persons are taken as test image to compute FRR and TSR. The remaining seven persons out of twenty two persons are considered as out of database to compute FAR.



FIGURE 5: Samples of Indian female database face images

3.2 Discrete Wavelet Transform

It serves as one of the important tools for image compression due to their data reduction capability. It analyses the signal at different frequency bands with different resolution by decomposition using high and low pass filters.

The Two Dimensional-Discrete Wavelet Transform (2D-DWT) is a multilevel decomposition technique that converts the images from spatial to frequency domain [15]. One-level of wavelet decomposition produces four filtered and sub sampled images referred to as sub bands. 2D-DWT is implemented as a convolution of selected wavelet function with the original image or it can be viewed as a set of two matrices of filters with row and columns. The mathematical representation of decomposition is given in equation (1).

$$C_f = X \times I \times Y \text{ ----- (1)}$$

Where,

C_f is the final matrix of wavelet coefficients

I is the original image

X is the matrix of row filters

Y is the matrix of column filters.

Figure 6 shows two levels of 2D filter tree [16]. The input image in each level is split into four bands using the low pass and high pass wavelet filters on the rows and columns. The row filters in each level are used to convert an image into low and high frequency components. The column filters in each level are used to convert low frequency components of row filters into low and high frequency components. Similarly high frequency components of row filters are converted into low and high frequency components. In each level four sub bands are generated. The low frequency sub bands of level 1 act as input to the level 2.

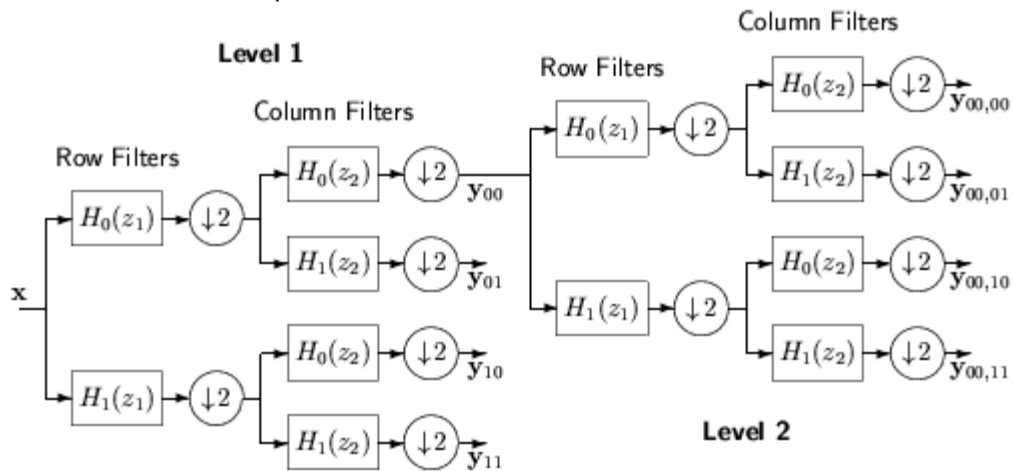


FIGURE 6: 2D DWT decomposition into two levels.

3.3 Laplacian Filter

It is used for image edge detection. The laplacian filter is applied on resized LL band coefficients of DWT. The original image coefficients are subtracted from laplacian filter coefficients to generate sharpened image.

3.4 Compound Local Binary Pattern (CLBP)

It is an extension of the Local Binary Pattern (LBP) texture operator. The image is converted into number of cells of dimension 3*3. The centre pixel in the 3*3 cell is considered as reference to generate CLBP texture operator with LSB for magnitude component and MSB for sign component. An example of CLBP texture operator for 3*3 image is shown in Figure 7. The intensity value of centre pixel is say I_c and intensity values of surrounded pixels are represented by I_p .

The sign component of CLBP is generated using equation (2)

$$CLBP_Sign = \begin{cases} 0 & : I_p - I_c \leq 0 \\ 1 & : I_p - I_c > 0 \end{cases} \dots\dots\dots (2)$$

The magnitude components of CLBP are generated using equation (3)

$$CLBP_Mag = \begin{cases} 0 & : I_p - I_c \leq M_{avg} \\ 1 & : I_p - I_c > M_{avg} \end{cases} \dots\dots\dots (3)$$

Where,

$$M_{avg} = (|m1| + |m2| + \dots + |m8|) / 8$$

$m1$ to $m8$ are the magnitude values of difference between respective I_p and I_c .

Example: Fig (a) is the original image, the intensity value difference between centre pixel and neighbouring pixels are given in fig (b). The sign component and magnitude components with CLBP are given in figures (c), (d) and (e) respectively. The binary 8 bits of sign and magnitude of each pixel are converted into decimal values to generate sign and magnitude features. The binary 8 bits of sign and magnitude of each pixel are converted into decimal values for feature extraction. The numbers of magnitude and sign components of CLBP for an image size of 256*256 are 64512.

$$M_{avg} = \frac{16 + 13 + 9 + 3 + 11 + 39 + 74 + 15}{8} = \frac{200}{8} = 25$$

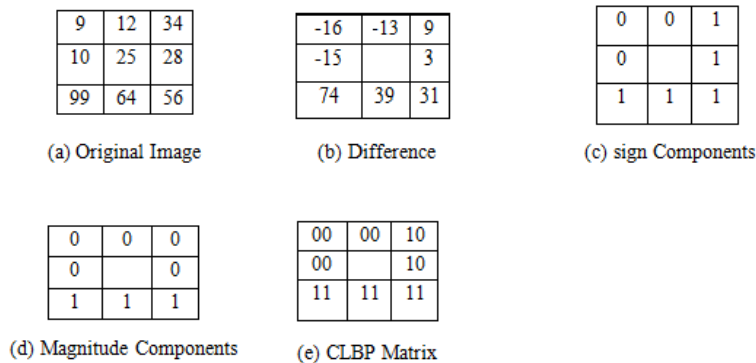


FIGURE 7: CLBP Operator.

3.5 Histogram

Histogram or specifically image histogram is the representation of an image in terms of a bar graph of pixel intensities. Histogram is a powerful tool used to view the image contrast and intensity distribution [17]. The histogram for image consists of pixel intensities plotted along the x-axis and the frequency of these pixel intensities along the y-axis. The histogram reduces number of features, which is advantage in real time application.

Example: - Consider an image of size 256 × 256 as shown in Figure 8. The total number of pixels in the image is 65536 with intensity levels varying from 0 to 255. The histogram of an image is shown in Figure 8. The histogram is applied on magnitude and sign components of CLBP to generate histogram features. The number of CLBP features are reduced from 64512 to 256, which increases the processing speed in real time applications. The histogram features of magnitude and sign components of CLBP are fused by concatenation to form CLBP – histogram features which are represented by C.

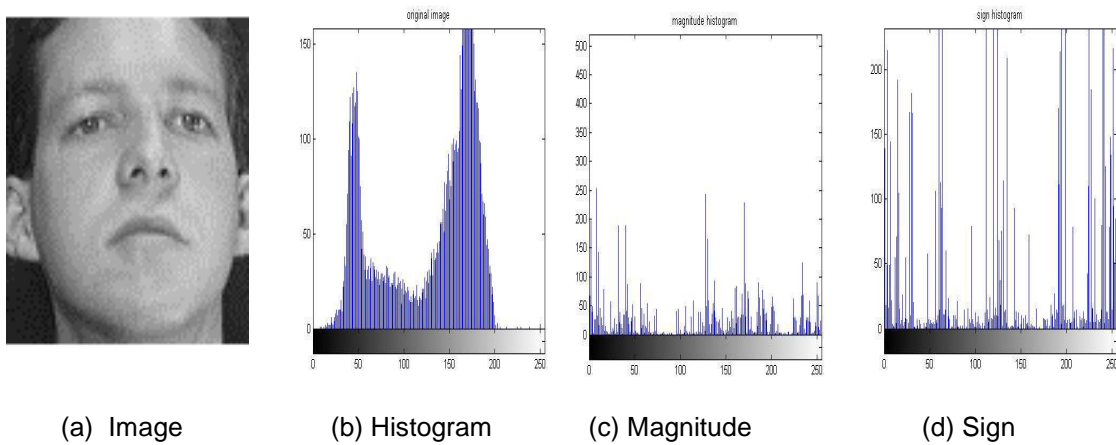


FIGURE 8: Histogram of original face image and CLBP.

3.6 Fast Fourier Transform (FFT)

The tool used to decompose an image into cosine (real) and sine (imaginary) components [18]. The transformation is the representation of input image into frequency domain. FFT algorithm is based on either divide and conquers method or linear filtering. The divide and conquer method includes FFT algorithms like Radix-2 and Radix-4 uses Decimation in Time (DIT) and Decimation in Frequency (DIF). FFT facilitates computation of Discrete Fourier Transform (DFT) in real time which reduces the complexity and reduces the computational time. The FFT and its inverse of 2D image can be computed using the equations (4) and (5).

$$\text{DFT: } F(x, y) = \sum_{m=0}^{M-1} \sum_{n=0}^{N-1} f(m, n) e^{-j2\pi(x\frac{m}{M} + y\frac{n}{N})} \text{----- (4)}$$

$$\text{IDFT: } f(m, n) = \frac{1}{MN} \sum_{x=0}^{M-1} \sum_{y=0}^{N-1} F(x, y) e^{j2\pi(x\frac{m}{M} + y\frac{n}{N})} \text{----- (5)}$$

Where,
M is the number of rows
N is the number of columns

It is observed from the equations (4) and (5) that the implementation is complex and expensive. Hence the 2D transform is split as two 1D transforms, one in horizontal direction and the other in

the vertical direction. The end result is equivalent to 2D transform in frequency domain. The 1-D DFT and IDFT are given in equations (6) and (7).

$$F(x) = \sum_{n=0}^{N-1} f(n)e^{-j2\pi(x\frac{n}{N})} \dots\dots\dots (6)$$

$$f(n) = \frac{1}{N} \sum_{x=0}^{N-1} F(x)e^{j2\pi(x\frac{n}{N})} \dots\dots\dots (7)$$

The magnitude values of F(X) are very high compared to pixel intensity values in the spatial domain and features are represented by D.

3.7 Fusion

The texture features are fused with transform domain features to generate final features. The final fusion features differentiate different and similar images efficiently compared to individual features. The CLBP-Histogram features and FFT magnitudes are fused using equation (8) to generate final features of an image.

$$Final\ Score\ F = P * D + (1 - P) * C \dots\dots\dots (8)$$

Where P is improved factor varies from 0 to 1
 D is transform domain features
 C is CLBP-histogram features.

3.8 Euclidian Distance

The final features of test images are compared with final features of images in the data base using Euclidian Distance (ED) to identify a person using equation (9).

$$E\ D = \sqrt{\sum_{i=1}^M (P_i - q_i)^2} \dots\dots\dots (9)$$

Where, M = No of coefficients in a vector.
 P_i = Coefficients values of vectors in database.
 q_i = Coefficient values of vectors in test image

4. ALGORITHM

Problem Definition: The hybrid domain technique is used for face recognition with DWT in the Preprocessing.

- The objectives are
- i) To increase TSR
 - ii) To decrease FRR, FAR and EER

The proposed face recognition algorithm using DWT, Filtering, CLBP, Histogram and FFT is given in Table 1.

TABLE 1: Proposed Algorithm.

<p>Input: Face Images Output: Performance parameters</p> <ol style="list-style-type: none"> 1. The Face Images are pre-processed using DWT, resize, filtering and subtract. 2. The CLBP is applied on preprocessed face images to generate magnitude and sign components. 3. The Histogram is applied on magnitude and sign components of CLBP and concatenate the Histograms of magnitude and sign. 4. The FFT is applied on preprocessed image to generate FFT magnitude features. 5. The FFT magnitude features are fused with concatenated histogram features to generate final features. 6. The final features of test and data base images are compared using Euclidian Distance. 7. Compute performance parameters such as TSR, FRR, FAR and EER.
--

5. PERFORMANCE ANALYSIS

In this section the definitions of performance parameter and performance analysis of proposed model are discussed.

5.1 Definitions of Performance Parameters

(i) **False Acceptance Rate:** The number of unauthorized persons accepted as authorized persons. It is the ratio of the number of unauthorized persons accepted to the total number of persons in the outside database and given in equation (10)

$$FAR = \frac{\text{Number of unauthorised persons accepted}}{\text{Total number of persons in the out of data base}} \dots\dots\dots (10)$$

(ii) **False Rejection Rate:** The number of authorized persons rejected as unauthorized persons. It is the ratio of number of authorized persons rejected to the total no of persons in the database as given in equation (11)

$$FRR = \frac{\text{Number of authorised persons rejected}}{\text{Total number of persons in the data base}} \dots\dots\dots (11)$$

(iii) **Total Success Rate:** The number of authorized persons recognized correctly in the database. It is the ratio of number of persons correctly matched to the total no of persons in the database and is given in equation (12)

$$TSR = \frac{\text{Number of persons correctly matched}}{\text{Total number of persons in the data base}} \dots\dots\dots (12)$$

(iv) **Equal Error Rate:** It is the measure of trade-off between FAR and FRR and is given in equation (13).

$$EER = FAR = FRR \dots\dots\dots (13)$$

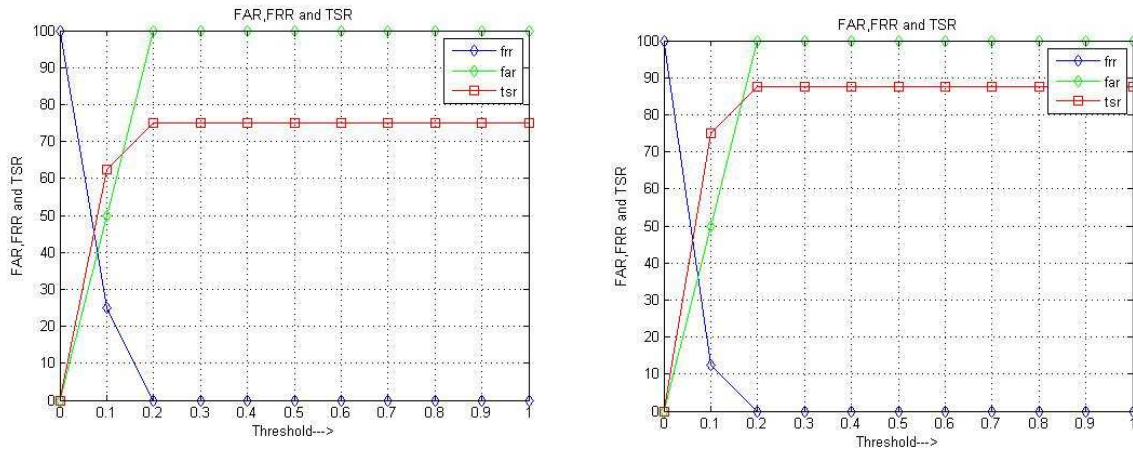
5.2 Analysis of Performance Parameter

The Performance Parameters such as FRR, FAR, EER and TSR for different face databases viz., JAFFE, ORL, Indian male and Indian female are discussed in detail for the proposed model.

5.2.1 Analysis using JAFFE Database

(i) CLBP Technique

The database is created to test the performance of an algorithm by considering eight persons inside data base and two persons outside data base. The variations of FAR, FRR and TSR with threshold using CLBP technique with/without Preprocessing are shown in Figure 9. The values of FRR decrease from 100 % to 0 % as threshold increases. The values of FAR and TSR increases with threshold. The values of Maximum TSR (Max.TSR) are 75 % to 87.5 % without and with preprocessing respectively. The EER values are less with preprocessing compared to without preprocessing.



(a) Without Preprocessing

(b) With Preprocessing

FIGURE 9: The variations of FAR, FRR and TSR with threshold for CLBP technique.

(ii) FFT Technique

The data base is created to test the performance of an algorithm by considering eight persons inside data base and two persons outside data base. The variations of FAR, FRR and TSR with threshold using CLBP technique with/without Preprocessing are shown in Figure 10. The values of FRR decrease for 100% to 0% as threshold increases. The values of FAR and TSR increases with threshold. The values of Max.TSR without and with Preprocessing are 100%. The EER values are less with preprocessing compared to without preprocessing.

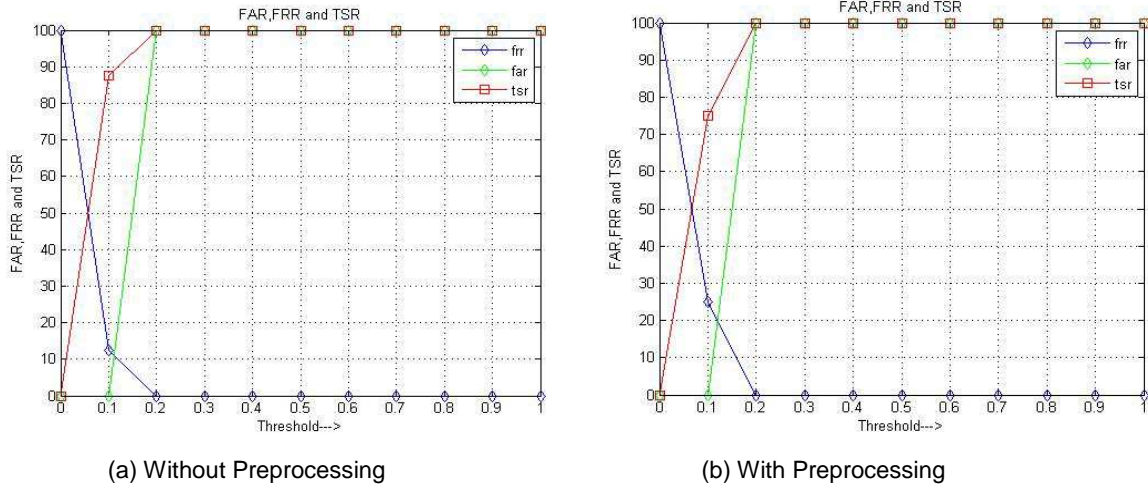


FIGURE 10: The variations of FAR, FRR and TSR with threshold for FFT technique.

(iii) Proposed Hybrid Technique

The data base is created to test the performance of an algorithm by considering eight persons inside data base and two persons outside data base. The variations of FAR, FRR and TSR with threshold using CLBP technique with/without Preprocessing are shown in Figure 11. The Values of FRR decrease for 100 % to 0 % as threshold increases. The values of FAR and TSR increases with threshold. The values of Max. TSR are 88.33% to 100% without and with preprocessing respectively. The EER values are less with Preprocessing compared to without Preprocessing.

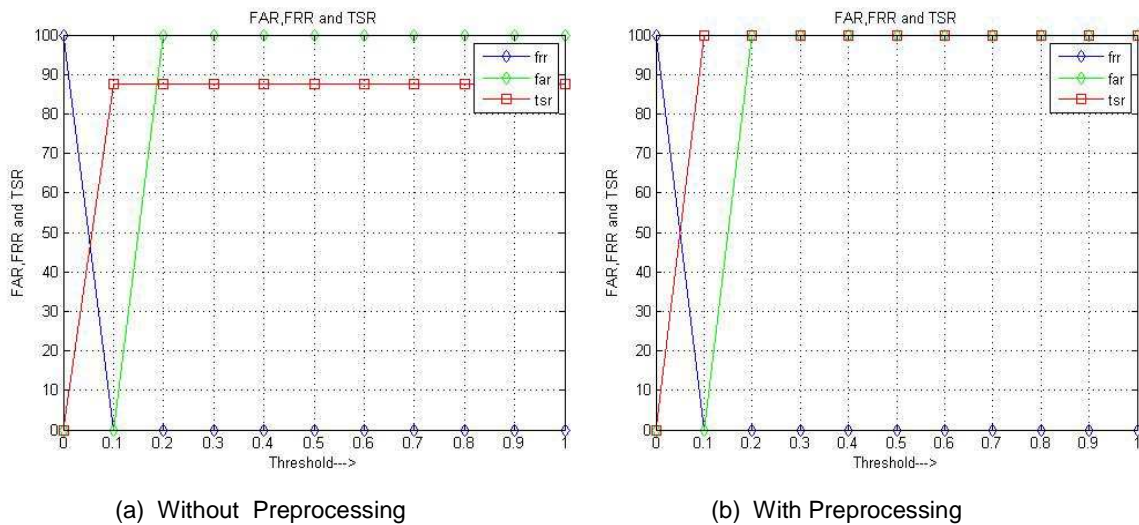


FIGURE 11: The variations of FAR, FRR and TSR with threshold for Hybrid technique.

(iv) Performance Comparison of CLBP, FFT and Hybrid Techniques

The performance parameters viz., EER, Optimum TSR (Opt.TSR) and Maximum TSR (Max.TSR) for CLBP, FFT and Hybrid domain techniques are tabulated in Table 2. The values of EER with Preprocessing are lower compared to without preprocessing. In all the three techniques the values of Max.TSR and Opt.TSR values are higher in the case of with preprocessing compared

to without preprocessing It is observed that the values EER are zero in the case proposed hybrid technique compared to CLBP and FFT techniques. The values Opt. and Max. TSR with and without preprocessing are high in the case of hybrid technique compared to CLBP and FFT techniques.

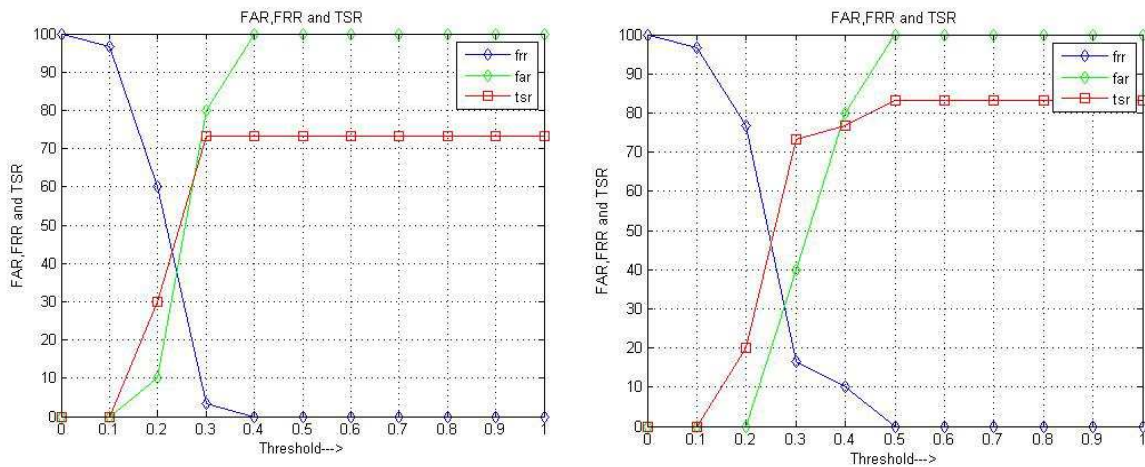
TABLE 2: Percentage variations of FAR, FRR and TSR without and with preprocessing.

Techniques	CLBP			FFT			Hybrid Technique		
	EER (%)	Opt. TSR (%)	Max. TSR (%)	EER (%)	Opt. TSR (%)	Max. TSR (%)	EER (%)	Opt. TSR (%)	Max. TSR (%)
Without preprocessing	40	50	75	20	80	100	0	88.33	88.33
With preprocessing	36	55	87.5	12	90	100	0	100	100

5.2.2 Analysis using ORL Database

(i) CLBP Technique

The data base is created to test the performance of an algorithm by considering thirty persons inside data base and ten persons outside data base. The variations of FAR, FRR and TSR with threshold using CLBP technique with/without Preprocessing are shown in figure 12. The values of FRR decrease for 100 % to 0 % as threshold increases. The values of FAR and TSR increases with threshold. The values of Max. TSR are 73.33 % to 83.33 % without and with Preprocessing respectively. The EER values are less with Preprocessing compared to without Preprocessing.



(a) Without Preprocessing

(b) With Preprocessing

FIGURE 12: The variations of FAR, FRR and TSR with threshold for CLBP technique.

(ii) FFT Technique

The data base is created to test the performance of an algorithm by considering thirty persons inside data base and ten persons outside data base. The variation of FAR, FRR and TSR with threshold using CLBP technique with/without Preprocessing is shown in Figure 13. The values of FRR decrease for 100% to 0% as threshold increases. The values of FAR and TSR increases

with threshold. The values of Max. TSR is 90% without and with Preprocessing. The EER values are less with preprocessing compared to without preprocessing

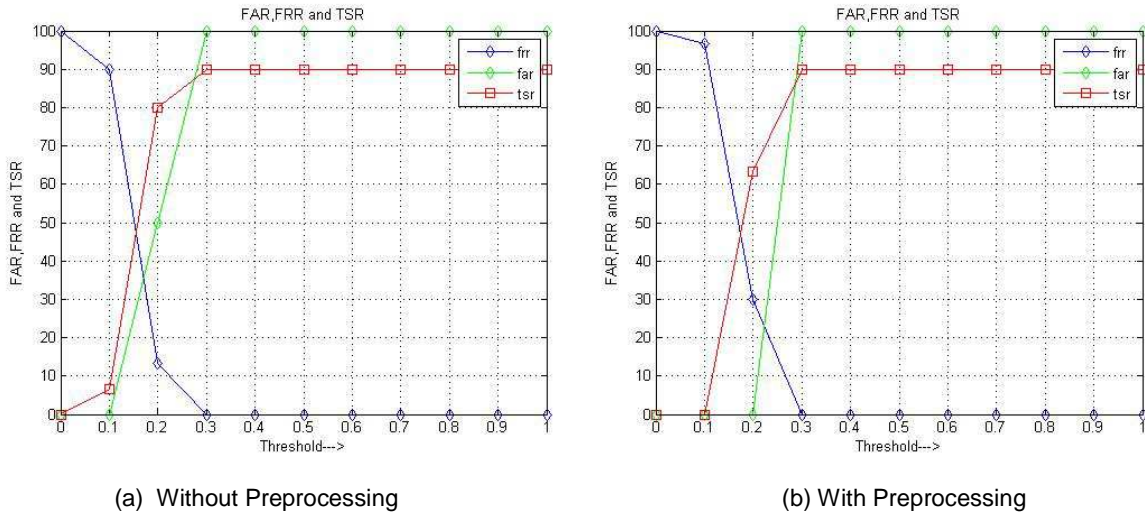


FIGURE 13: The variations of FAR, FRR and TSR with threshold for FFT technique.

(iii) Proposed Hybrid Technique

The data base is created to test the performance of an algorithm by considering thirty Persons Inside Data base and ten Persons Outside Data base. The variations of FAR, FRR and TSR with threshold using CLBP technique with/without Preprocessing are shown in Figure 14. The values of FRR decrease for 100 % to 0 % as threshold increases. The values of FAR and TSR increases with threshold. The values of Max. TSR are 93.33% without and with Preprocessing. The EER values are less with preprocessing compared to without preprocessing.

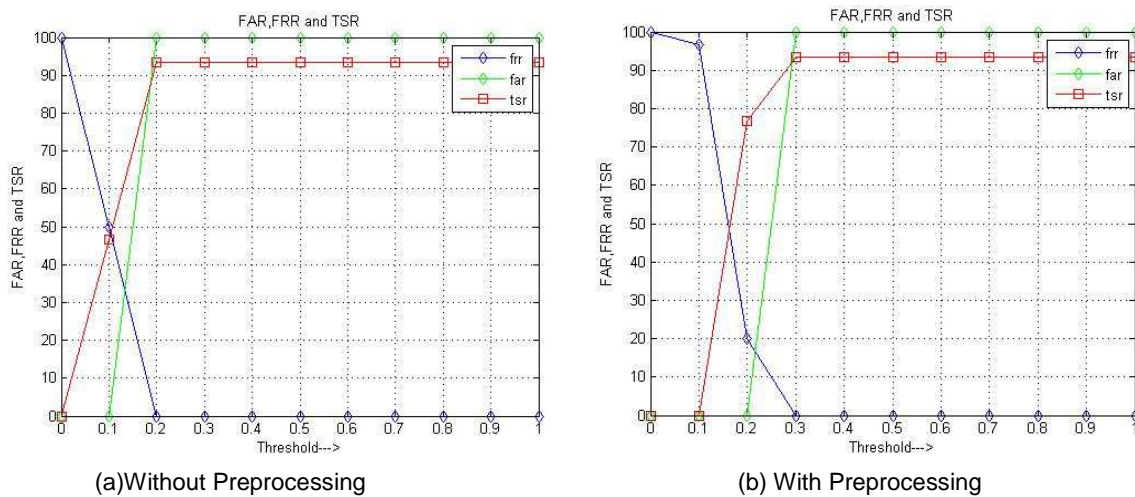


FIGURE 14: The variations of FAR, FRR and TSR with threshold for Hybrid technique.

(iv) Performance Comparison of CLBP, FFT and Hybrid Techniques

The performance parameters viz., EER, Optimum TSR and Maximum TSR for CLBP, FFT and Hybrid domain techniques are tabulated in Table 3. The values of EER with preprocessing are lower compare to without preprocessing. In all the three techniques the values of Max.TSR and opt. TSR values are higher in the case of with preprocessing compared to without preprocessing. It is observed that the values EER are zero in the case proposed hybrid technique compare to CLBP and FFT techniques. The values opt. and Max.TSR with and without preprocessing are high in the case of hybrid technique compared to CLBP and FFT techniques.

TABLE 3: Percentage variations of FAR, FRR and TSR without and with preprocessing.

Techniques	CLBP			FFT			Hybrid Technique		
	EER (%)	Opt. TSR (%)	Max. TSR (%)	EER (%)	Opt. TSR (%)	Max. TSR (%)	EER (%)	Opt. TSR (%)	Max. TSR (%)
Without preprocessing	40	45	73.33	20	60	90	32	60	93.33
With preprocessing	30	60	83.33	12	68	90	18	80	93.33

5.2.3 Analysis using Indian Male Database

(i) CLBP Technique

The data base is created to test the performance of an algorithm by considering twelve Persons inside Data base and eight Persons Outside Data base. The variation of FAR, FRR and TSR with threshold using CLBP technique with/without Preprocessing is shown in Figure 15. The values of FRR decrease for 100 % to 0 % as threshold increases. The values of FAR and TSR increases with threshold. The values of Max. TSR are 66.66 % to 83.33 % without and with Preprocessing respectively. The EER values are less with preprocessing compared to without preprocessing.

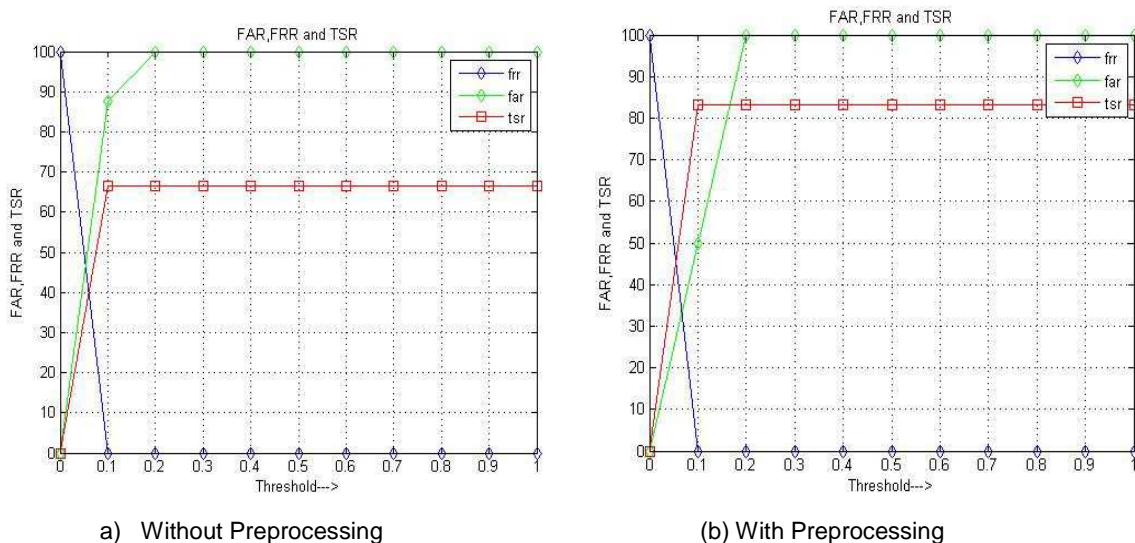


FIGURE 15: The variations of FAR, FRR and TSR with threshold for CLBP technique.

(ii) FFT Technique

The data base is created to test the performance of an algorithm by considering twelve Persons inside Data base and eight Persons outside Data base. The variations of FAR, FRR and TSR with threshold using CLBP technique with/without Preprocessing are shown in Figure 16. The values of FRR decrease for 100% to 0% as threshold increases. The values of FAR and TSR increases with threshold. The values of Max. TSR are 72% to 80% without and with Preprocessing respectively. The EER values are less with preprocessing compared to without preprocessing

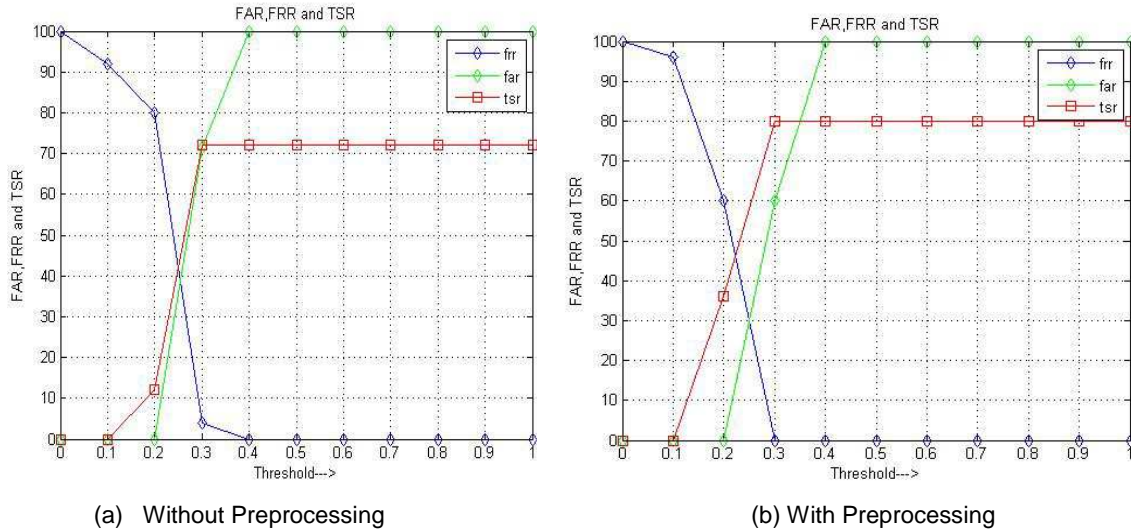


FIGURE 16: The variations of FAR, FRR and TSR with threshold for FFT technique.

(iii) Proposed Hybrid Technique

The data base is created to test the performance of an algorithm by considering eight Persons Inside Data base and two Persons Outside Data base. The variations of FAR, FRR and TSR with threshold using CLBP technique with / without Preprocessing are shown in Figure 17. The values of FRR decrease for 100 % to 0 % as threshold increases. The values of FAR and TSR increases with threshold. The values of Max.TSR without and with Preprocessing are 100%. The EER values are less with preprocessing compared to without preprocessing.

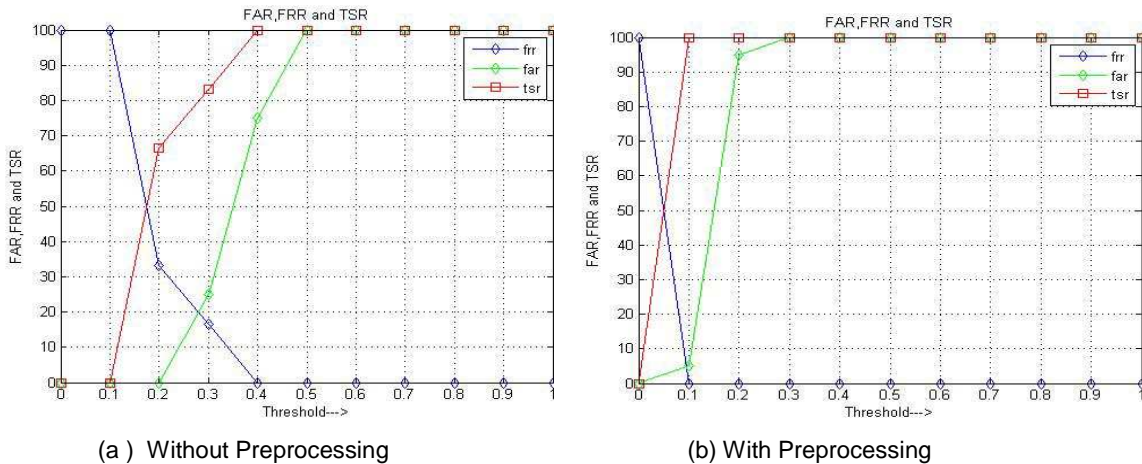


FIGURE 17: The variations of FAR, FRR and TSR with threshold for Hybrid technique.

(iv) Performance Comparison of CLBP, FFT and Hybrid Techniques

The performance parameters viz., EER, optimum TSR and maximum TSR for CLBP, FFT and Hybrid domain techniques are tabulated in Table 4. The values of EER with preprocessing are lower compared to without preprocessing. In all the three techniques the values of Max. TSR and opt. TSR values are higher in the case of with preprocessing compared to without preprocessing. It is observed that the values EER are zero in the case proposed hybrid technique compared to CLBP and FFT techniques. The values opt. and Max.TSR with and without preprocessing are high in the case of hybrid technique compared to CLBP and FFT techniques.

TABLE 4: Percentage variations of FAR, FRR and TSR without and with preprocessing.

Techniques	CLBP			FFT			Hybrid Technique		
	EER (%)	Opt. TSR (%)	Max. TSR (%)	EER (%)	Opt. TSR (%)	Max. TSR (%)	EER (%)	Opt. TSR (%)	Max. TSR (%)
Without preprocessing	48	50	66.66	40	43	72	20	80	100
With preprocessing	32	56	83.33	30	60	80	4	100	100

5.2.4 Analysis using Indian Female Database

(i) CLBP Technique

The data base is created to test the performance of an algorithm by considering fifteen persons inside data base and seven persons outside data base. The variation of FAR, FRR and TSR with threshold using CLBP technique with / without Preprocessing is shown in Figure 18. The values of FRR decrease for 100 % to 0 % as threshold increases. The values of FAR and TSR increases with threshold. The values of Max.TSR are 60 % to 72.11 % without and with Preprocessing respectively. The EER values are less with preprocessing compared to without preprocessing.

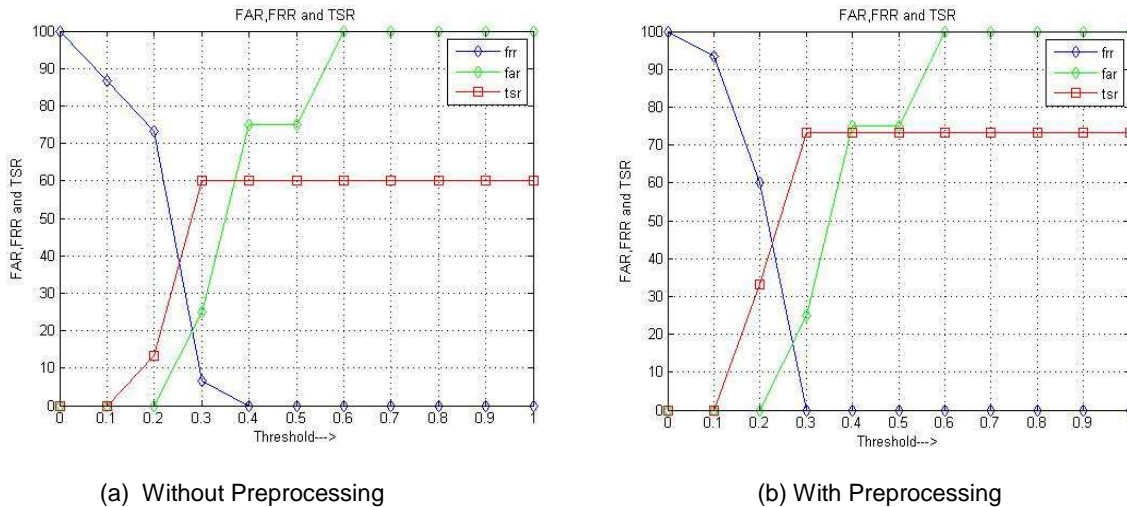


FIGURE 18: The variations of FAR, FRR and TSR with threshold for CLBP technique.

(ii) FFT Technique

The data base is created to test the performance of an algorithm by considering fifteen persons inside data base and seven persons outside data base. The variations of FAR, FRR and TSR with threshold using CLBP technique with / without Preprocessing are shown in Figure 19. The values of FRR decrease for 100% to 0% as threshold increases. The values of FAR and TSR increases with threshold. The values of Max. TSR are 60% to 72.11 without and with Preprocessing. The EER values are less with preprocessing compared to without preprocessing

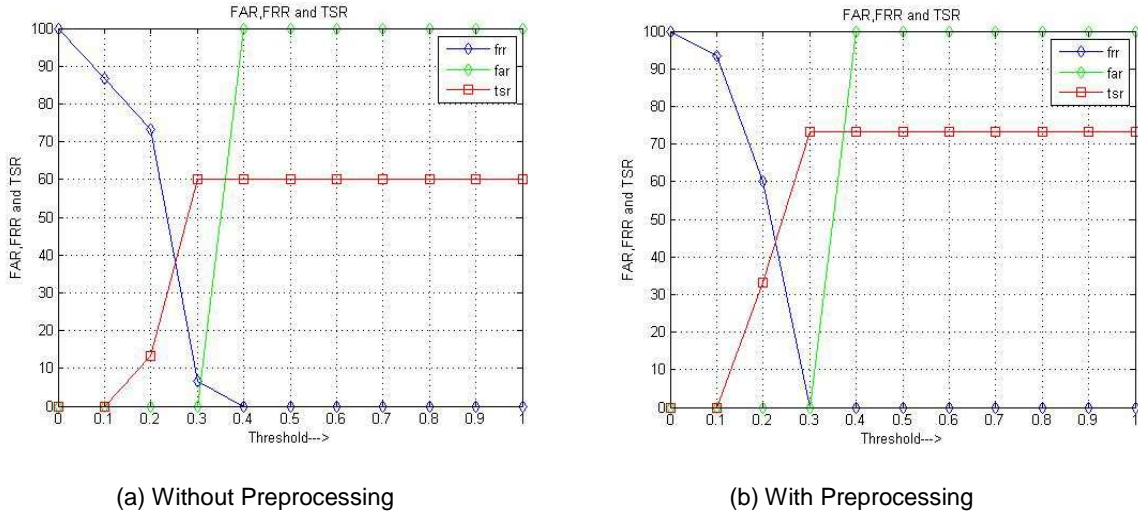


FIGURE 19: The variations of FAR, FRR and TSR with threshold for FFT technique.

(iii) Proposed Hybrid Technique

The data base is created to test the performance of an algorithm by considering fifteen persons inside data base and seven persons outside data base. The variations of FAR, FRR and TSR with threshold using CLBP technique with / without Preprocessing are shown in figure 20. The values of FRR decrease for 100 % to 0 % as threshold increases. The values of FAR and TSR increases with threshold. The values of Max.TSR are 86.46% to 93.33% without and with Preprocessing respectively. The EER values are less with preprocessing compared to without preprocessing.

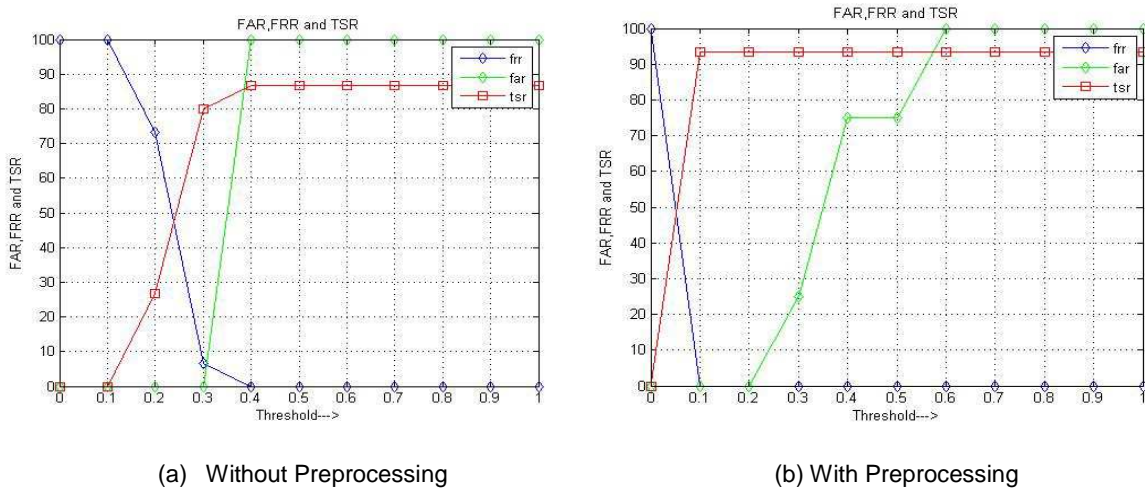


FIGURE 20: The variations of FAR, FRR and TSR with threshold for Hybrid technique.

(iv) Performance comparison of CLBP, FFT and Hybrid Techniques

The performance parameters viz., EER, optimum TSR and maximum TSR for CLBP, FFT and Hybrid domain techniques are tabulated in Table 5. The values of EER with preprocessing are lower compare to without preprocessing. In all the three techniques the values of Max. TSR and opt. TSR values are higher in the case of with preprocessing compared to without preprocessing. It is observed that the values EER are zero in the case proposed hybrid technique compare to CLBP and FFT techniques. The values opt. and Max.TSR with and without preprocessing are high in the case of hybrid technique compared to CLBP and FFT techniques.

TABLE 5: Percentage variations of FAR, FRR and TSR without and with preprocessing.

Techniques	CLBP			FFT			Hybrid Technique		
	EER (%)	Opt. TSR (%)	Max. TSR (%)	EER (%)	Opt. TSR (%)	Max TSR (%)	EER (%)	Opt TSR (%)	Max TSR (%)
Without preprocessing	20	50	60	5	60	60	5	80	86.46
With preprocessing	18	60	72.11	0	72.11	72.11	0	93.33	93.33

5.2.5 Comparison of Proposed Algorithm with Existing Algorithms for ORL Database

The percentage TSR of proposed algorithm for ORL database is compared with existing algorithm presented by Pallavi D. Wadakar and Megha Wankhade [19], Swarup Kumar Dandpat and Sukadev Meher [20] and D Murugan et al.,[21] and is given in Table 6. It is observed that the percentage TSR is high in the case of proposed algorithm since the combination of DWT, CLBP and FFT techniques are used compared to DWT, PCA+2DPCA and DWT+PCA techniques used in the existing algorithms. The performance parameter values are computed to demonstrate the proposed algorithm is better for the following reasons. (i) The face images are preprocessed using DWT and Laplacian filter to generate sharpened face images.(ii)The CLBP magnitude and sign component produce texture feature which represents micro level information and also produce high dimensional features which results in better performance parameters.(iii)The histogram on CLBP features reduces high dimensional features to low dimensional features.(iv)The FFT magnitude features are able to produce highly discriminant features for images of different persons.(v)The proposed algorithm is able to produce highly similar features for images of same persons and highly discriminant features for images of different persons. This is proved through Euclidian Distance and experimental results.

TABLE 6: Comparison of TSR with proposed and existing algorithms.

SI No	Authors	Techniques	Max.TSR (%)
1	Pallavi D. Wadakar and Megha Wankhade[19]	DWT	90
2	Swarup Kumar Dandpat and Sukadev Meher [20]	PCA+2DPCA	90.5
3	D Murugan et al.,[21]	Gabor filter + DWT + PCA	92
4	Proposed Method	DWT + CLBP+FFT	93.33

6. CONCLUSION

The biometrics are used to create human data base of nation for authentication and national security. In this paper Hybrid Domain based Face Recognition using DWT, FFT and Compressed CLBP is proposed. The face data bases are preprocessed using LL band of DWT and Laplacian filter to generate sharpened face images. The CLBP is applied on sharpened face images to generate high dimensional magnitude and sign features. The histogram is applied on magnitude and sign features to convert high dimensional features to low dimensional features. The FFT is applied on sharpened face images to generate FFT magnitude features. The low dimensional histogram features are fused with high dimensional FFT magnitude features using strengthening equation to generate final features. The data base image features and test image features are compared using ED to compute performance parameters. The performance parameter values are better in the case of proposed algorithm compared to existing algorithms. In future the algorithm can be tested using FPGA which suits real time applications.

7. REFERENCES

- [1] Faisal R. Al-Osaimi, Mohammed Bennamoun and Ajmal Main, "Spatially optimized Data-Level Fusion of Texture and Shape for Face Recognition," IEEE Transactions on Image Processing, Vol. 21, No.2, pp 859 -872 ,2012.
- [2] Raghuraman Gopalan, Simha Taheri, Pavan Turaga, Rama Challappa, "A Blur-Robust Descriptor with Applications to Face Recognition," IEEE Transactions on Pattern Analysis and Machine Intelligence, Vol 34, No 6, pp.1220-1226, 2012.
- [3] Ping-Han Lee, Szu-Wei Wu and Yi-Ping Hung "Illumination Compensation using Oriented Local Histogram Equalization and Its Application to Face Recognition," IEEE Transactions on Image processing, Vol 21, No 9, pp. 4280-4289, 2012.
- [4] Timo Ahonen, Abdenour Hadid and Matti Pietikainen, "Face Description with Local Binary Patterns: Application to Face Recognition," IEEE Transactions on pattern analysis and Machine intelligence, Vol 28, No. 12, pp. 2037-2041, 2006.
- [5] Parama Bagchi, Debotosh Bhattacharjee and Mita Nasipuri " Robust 3D Recognition in Presence of Pose and Partial Occlusions or Missing Parts," International Journal in Foundations of Computer Science and Technology, Vol. 4, No.4, pp. 21-35, 2014.
- [6] Michel F. Valstar and Maja Pantic, "Fully Automatic Recognition of the Temporal Phases of Facial Actions," IEEE Transactions on systems, Man, and Cybernetics-Part B: Cybernetics, Vol-42, No. 1, pp. 28-42, 2012.
- [7] Wilman W.W. Zou, and Pong C.Yuen "Very Low Resolution Face Recognition Problem," IEEE Transactions on Image Processing, Vol. 21, No. 1, pp.327-340, 2012.
- [8] Hu Han, Charles Otto, Xiaoming Liu and Anil K. Jain, "Demographic Estimation from Face Images: Human Vs. Machine Performance," IEEE Transactions on Pattern Analysis and Machine Intelligence, pp.1-14, 2014.
- [9] Changxing Ding, Chang Xu and Dacheng Tao "Multi-Task Pose-Invariant Face Recognition," IEEE Transactionson Image Processing, Vol. 24, No. 3, pp. 980-992, 2015.
- [10] Faisal Ahmed, Emam Hossain, A.S.M. Hossain Bari and ASM Shihavuddin, "Compound Local Binary Pattern (CLBP) for Robust Facial Expression Recognition," IEEE International Symposium on Computational Intelligence and Informatics, pp.391-395, Budapest, Hungary, 2011.

- [11] Jae Young Choi, Yong Man Ro and Konstantinos N. Plataniotis "Color Local Texture Features for Color Face Recognition" IEEE Transactions on Image Processing, Vol. 21, No. 3, pp.1366-1380, 2012.
- [12] Jaffe Database, http://www.kasrl.org/jaffe_download.html.
- [13] ORL database, <http://www.camrol.co.uk>
- [14] Indian Face Database, <http://viswww.cs.umass.edu/~vidit/Indian Face Database>
- [15] J. Petrova, E. Ho-s-talkova, "Edge Detection in Medical Images using the Wavelet Transform," Department of Computing and Control Engineering, Institute of Chemical Technology, Prague, Technicka 6, 16628 Prague 6, Czech Republic, 2011.
- [16] 2-D-DWT, <http://cnx.org/contents/a53d13be-b4f1-47c7-a783-dc965f5e945d@4/The-2-D-DWT>
- [17] Madhulakshmi, Abdul Wahid Ansari, "Face Recognition Using Featured Histogram," International Journal of Emerging Technology and Advanced Engineering Vol 3, Issue 8, pp.142- 147, 2013.
- [18] http://www.gamasutra.com/view/feature/132385/sponsored_feature_implementation.php
- [19] Pallavi D.Wadkar and MeghaWankhade, "Face Recognition using Discrete Wavelet Transforms," International Journal of AdvancedEngineering Technology, vol. 3, pp. 239-242, 2012.
- [20] Swarup Kumar Dandapat and Sukadev Meher, "Performance Improvement for Face Recognition using PCA and Two-Dimensional PCA," IEEE International Conference on Computer Communication and Informatics, pp. 1-5, 2013.
- [21] D Murugan, S Arumugam, K Rajalakshmi and Manish T, "Performance Evaluation of Face Recognition using Gabor Filter, Log Gabor filter and Discrete Wavelet Transform," International Journal of computer science and Information Technology, vol. 2, no. 1, pp. 125-133, 2010.

INSTRUCTIONS TO CONTRIBUTORS

The *International Journal of Image Processing (IJIP)* aims to be an effective forum for interchange of high quality theoretical and applied research in the Image Processing domain from basic research to application development. It emphasizes on efficient and effective image technologies, and provides a central forum for a deeper understanding in the discipline by encouraging the quantitative comparison and performance evaluation of the emerging components of image processing.

We welcome scientists, researchers, engineers and vendors from different disciplines to exchange ideas, identify problems, investigate relevant issues, share common interests, explore new approaches, and initiate possible collaborative research and system development.

To build its International reputation, we are disseminating the publication information through Google Books, Google Scholar, Directory of Open Access Journals (DOAJ), Open J Gate, ScientificCommons, Docstoc and many more. Our International Editors are working on establishing ISI listing and a good impact factor for IJIP.

The initial efforts helped to shape the editorial policy and to sharpen the focus of the journal. Started with Volume 9, 2015, IJIP will be appearing with more focused issues. Besides normal publications, IJIP intends to organize special issues on more focused topics. Each special issue will have a designated editor (editors) – either member of the editorial board or another recognized specialist in the respective field.

We are open to contributions, proposals for any topic as well as for editors and reviewers. We understand that it is through the effort of volunteers that CSC Journals continues to grow and flourish.

LIST OF TOPICS

The realm of International Journal of Image Processing (IJIP) extends, but not limited, to the following:

- Architecture of imaging and vision systems
- Character and handwritten text recognition
- Chemistry of photosensitive materials
- Coding and transmission
- Color imaging
- Data fusion from multiple sensor inputs
- Document image understanding
- Holography
- Image capturing, databases
- Image processing applications
- Image representation, sensing
- Implementation and architectures
- Materials for electro-photography
- New visual services over ATM/packet network
- Object modeling and knowledge acquisition
- Autonomous vehicles
- Chemical and spectral sensitization
- Coating technologies
- Cognitive aspects of image understanding
- Communication of visual data
- Display and printing
- Generation and display
- Image analysis and interpretation
- Image generation, manipulation, permanence
- Image processing: coding analysis and recognition
- Imaging systems and image scanning
- Latent image
- Network architecture for real-time video transport
- Non-impact printing technologies
- Photoconductors

- Photographic emulsions
- Prepress and printing technologies
- Remote image sensing
- Storage and transmission

- Photopolymers
- Protocols for packet video
- Retrieval and multimedia
- Video coding algorithms and technologies for ATM/p

CALL FOR PAPERS

Volume: 9 - Issue: 6

i. Submission Deadline : October 31, 2015

ii. Author Notification: November 30, 2015

iii. Issue Publication: December 2015

CONTACT INFORMATION

Computer Science Journals Sdn Bhd

B-5-8 Plaza Mont Kiara, Mont Kiara
50480, Kuala Lumpur, MALAYSIA

Phone: 006 03 6204 5627

Fax: 006 03 6204 5628

Email: cscpress@cscjournals.org

CSC PUBLISHERS © 2015
COMPUTER SCIENCE JOURNALS SDN BHD
B-5-8 PLAZA MONT KIARA
MONT KIARA
50480, KUALA LUMPUR
MALAYSIA

PHONE: 006 03 6204 5627

FAX: 006 03 6204 5628

EMAIL: cscpress@cscjournals.org